ON HEAT TRANSFER WITHIN AND ACROSS NEARLY CIRCULAR CAVITIES INCLUDING THE EFFECTS OF VARIABLE WALL TEMPERATURE AND MASS BLEED

By

ERVIN LYNN BALES
B.S., University of South Carolina, 1957
M.S., Bradley University, 1962

N10K

THESIS

Submitted in partial fulfillment of the requirements
for the degree of Doctor of Philosophy in Mechanical Engineering
in the Graduate College of the
University of Illinois, 1967

Urbana, Illinois

ACKNOWLEDGMENT

I express appreciation to Dr. H. H. Korst, the thesis adviser and committee chairman, for his incomparable counsel and guidance.

I wish to express deep thanks and gratitude to my wife, Julia, for voluntarily and to my three children, Steven, Kim and Karen, for involuntarily enduring the trials of my returning to graduate school from industry.

Thanks are also due Tom Degenhart for his meticulous construction of the heater controls.

The thesis project was supported by NASA Research Grant NsG 13-59.

PRECEDING PAGE BLANK NOT FILMED.

TABLE OF CONTENTS

I. INTRODUCTION

In recent years several investigators have become interested in flow separation induced by wall discontinuities and the resultant interaction between the external flow field and the wake. Such wakes may either be produced by front or rearward facing walls causing separation of the front-step or rear-step variety leading mainly to form drag problems, or they may be of the cavity variety, where an external stream interacts with the wake flow mainly through shear stresses in the mixing region. However, not only drag considerations but also heat transfer phenomena, especially in the region near flow reattachment to solid walls, have motivated experimental and theoretical studies. Cavity type geometries have been studied where the vortical motion inside the cavity, driven by the external flow field through a shear region, is well defined and can be subjected to quantitative analysis. Most of the previous investigators have presented empirical information and qualitative discussions of the nature of the flow and heat transfer but have not derived complete analytical models for the velocity field or the heat transfer in the cavity (14,16,17,18,28,29). The exception noted has been the work of Korst (1), Golik (3), and Miles (4) which is also considered and included in the present study as a particular case of the general analysis.

Generally two simple geometries have found the attention of the investigators, namely nearly circular or rectangular cavities. Each has its particular advantage. The rectangular model is easier to fabricate and may be easily changed in size by allowing a movable floor or wall. This is generally the model used by the workers who are primarily interested in an experimental investigation as it allows an easy variation of the geometrical parameters.

On the other hand, the nearly circular cavity with its sharp, well defined separation and reattachment edges eliminates secondary vortices that form in the corners between the walls and the bottom and which tend to complicate the flow picture. Variations of geometrical parameters in the experimental investigation is, however, somewhat more difficult especially if wall heating is to be accomplished. In particular, the predominance of a vortical flow in the cavity (approaching solid body rotation) and the rather well defined shear flow regions along the cavity boundaries (attached boundary layer along the wall and the free jet mixing region separating the cavity from the external flow field) make the nearly circular cavity most attractive for combined analytical and experimental studies.

It is well known that finite wake velocities do exist and must necessarily be considered to determine dissipation along the cavity wall and to account for any heat transfer to and across the separated flow region. Indeed, finite wake velocities not only are necessary for explaining heat transfer, but also control the balance between mechanical energy transferred to, and dissipated within the cavity; it is the very mechanism which sustains the velocities.

In an attempt to relate the academic interest in flows over cavities to practical engineering applications, two specific uses can be selected as being representative. (These could be extended to applications of a similar nature.)

External surface cavities on controlled flight space vehicles for surface temperature control could be advantageous for long duration, severe heating flights in the atmosphere. Such vehicles would be the manned skip-glide type once considered by one of the space programs. Ablation cooling, such as is presently used for manned re-entry flight, would be at a disadvantage for controlled re-entry due to the great and to some degree uncontrollable changes in body shape. Aerodynamically the body shape is of no great importance in present orbital missions as long as there is no structural failure, for there is no need for aerodynamic surfaces after re-entry. In future more sophisticated missions, as a return from the moon, the vehicle might be required to land under fully controlled flight which would preclude ablating surfaces and will necessitate some other method of surface cooling.

The results of the present analysis may be compared by the designer for given wall and mass bleed cooling rates for a cavity to the cooling of an equivalent non-isothermal flat plate and the advantage or disadvantage will be apparent for a given mission. No attempt is made to determine how wall cooling and/or mass injection might be accomplished in vehicle design, but the analytical results could be used to determine the best balance between the two cooling methods to achieve the most effective design.

Another possible use for surface cavities is the control of environmental temperature of external sensors, transducers or other external instrumentation on a high velocity vehicle flying in the atmosphere. The sensor could be placed in a protective cavity where the core region is maintained at the desired temperature level, no matter what the free stream conditions, by using an automatic control system.

The intent of the present thesis was to develop a useful mathematical model describing the flow field and heat transfer inside and over a nearly circular cavity with arbitrary wall temperature distribution and including effects of mass bleed into the cavity core region at an arbitrary total temperature. The model was derived for steady, incompressible, constant property, turbulent flow over a two-dimensional cavity. A systems analysis such as Korst, Golik and Miles used, delineated the individual parts of the complete flow field. The parts were then analyzed and interfaced to provide the complete cavity model. The dissipative aspects of the flow model established the velocity field on the basis of a mechanical energy balance. The general energy equation, with the aid of the now determined velocity field, was then used to calculate the convective heat transfer rates and establish a thermodynamic balance for the cavity.

II. ANALYSIS

Investigation of Korst (1), Golik (3), and Miles (4) have demonstrated the feasibility and usefulness of studying cavity flow by using a systems analysis whereby individual mechanisms of dissipation and energy transfer can be delineated and analyzed. The present work similarly uses a systems analysis to investigate the flow and heat transfer in a nearly circular cavity with internal mass bleed and a non-isothermal wall. The dissipative model is examined first and the velocity distributions in the shear regions are determined. These velocity distributions are then used in a heat transfer model in determining the temperature distribution and the accompanying heat transfer from and across the nearly circular cavity.

Each of these two models is divided into two dependent parts for analysis, the shear region across the cavity opening and the wake or vortical flow region within the cavity. The wake velocities not only establish the heat transfer mechanism within the cavity but also control a balance between the mechanical energy transferred to the cavity and that dissipated within the cavity. Thus the shear region is controlled by the wake which it sustains.

A. Dissipative Model

The dissipative model follows the systems method of analysis used by Korst (1) and Golik (3) in establishing the wake kinematics on the basis of a mechanical energy balance. The analysis was limited to a turbulent boundary layer at the point of separation at the leading edge of the cavity, a two-dimensional model, and steady flow. The shear region is assumed to completely span the cavity opening, that is the open cavity case as designated in the literature, references (28) and (3).

Charwat (28) and Maull (29) discuss the case of unsteady cavity flow and Miles (4) presents some estimates of the range of steady flow. Golik (3) defines the limits for an open cavity in terms of the ratio of cavity wall length to cavity opening length.

A mechanical energy balance may be made for any cavity shape but the particularizing of the resultant equations for a circular cavity will make apparent the advantage of that geometry. The systems' control surface and the nomenclature used in the analysis are indicated in figure 1. The boundaries are the "j" streamline which divides the fluid in or coming from within the cavity from that of the free stream, the solid wall of the cavity, and a closing cross section at reattachment between the "j" and "d" streamlines. The "d" streamline stagnates at the reattachment point R and separates the fluid leaving the cavity from that which recirculates within the cavity.

For mass bleeding into the cavity a mass efflux occurs between the "j" and "d" streamlines and requires from a conservation of mass that

$$G_s + \int_{y_j}^{y_d} \rho u \, dy = 0$$

Mechanical energy transferred to the system across the "j" streamline due to the shear work of the mixing region must equal the mechanical energy dissipated in the cavity and the efflux of kinetic energy due to mass bleed.

$$\int_0^{l_m} \tau_j u_j \, dy - \frac{1}{2} \int_{y_d}^{y_j} \rho u^3 \, dy = \int_V e_D \, dV$$

It is assumed that the dissipations may be identified and evaluated as individual terms which do not interact. These components are the total rates of dissipation in (1) the jet mixing region, E_{D_M} (2) the recompression zone, E_{D_R} (3) the cavity wall boundary layer, $E_{D_{BL}}$ and (4) the cavity core region, E_{D_C}. Therefore,

$$\int_V e_D \, dV = E_{D_M} + E_{D_R} + E_{D_{BL}} + E_{D_C}$$

To make the model more amenable to analysis a nearly circular shaped cavity was selected. This is a geometry which allows a discussion of the essential mechanisms but is simple enough to give meaning to both the theory and comparison with experiment. This choice reduces some of the dissipative terms to relatively small values and allows a meaningful analysis of the remaining terms. A discussion of the individual terms of the mechanical energy equation follows.

1. The jet mixing region--In determining the transfer of mechanical energy to the wake, it was convenient to define the net transfer of mechanical energy (reference 1)

$$E_T = \int_0^{l_m} \tau_j u_j \, dx - \frac{1}{2}\int_{y_d}^{y_j} \rho u^3 dy - E_{D_m}$$

Of course the evaluation of dissipation in the mixing zone is dependent on the solution of the jet mixing problem. As the velocity along the edge of the core flow region and the dissipative region is nearly constant, the shear region can be reasonably approximated by non-isoenergetic, turbulent jet mixing between two uniform streams at constant pressure. A discussion of the analysis of the flow in the shear region follows. The kinematic results are then used in calculating the dissipative terms in a mechanical energy balance. The temperature distributions determined in the shear region flow analysis are used later in the thermal energy balance of the heat transfer model.

Mathematical models for the mixing of two streams have been reported by several researchers for either the limiting case of a similarity solution or the more general case of a developing shear layer approaching similarity asymptotically (1-8). Both approaches are essentially momentum integral methods applied to velocity profiles which have been obtained as solutions for a highly simplified linearized equation of motion describing constant pressure mixing. A more generalized method although originally restricted to laminar mixing has been outlined by Pai (10).

Similarity Profiles As a first approximation a similarity solution was used by Korst and Golik. The results were satisfactory and a method was devised to account for the initial boundary layer in the primary stream using an "equivalent bleed" concept. The equation for a two-dimensional, constant pressure mixing region,

$$\rho u \frac{\partial u}{\partial x} + \rho v \frac{\partial u}{\partial y} = \frac{\partial}{\partial y}\left(\rho \nu \frac{\partial u}{\partial y}\right)$$

was linearized and solved for arbitrary initial conditions but special interest was centered on the "restricted case" of either large downstream distances or vanishing initial boundary layer thickness, for which the asymptotic error function profile was obtained (2).

$$\varphi = \frac{1+\varphi_b}{2} + \frac{1-\varphi_b}{2}\,\mathrm{erf}\,\eta$$

where

$$\varphi = \frac{u}{u_a}$$

$$\eta = \frac{\sigma y}{x}$$

$\sigma = f\left(C_a^2, \frac{T_{ob}}{T_{oa}}, \phi_b\right)$, an empirical parameter which is related to the rate of spreading of the mixing zone.

The restricted solution was obtained from the solution to the linearized equation with given initial flow profiles by allowing a "position parameter" to asymptotically approach zero (8).

The initial boundary layer may then be taken into account by introducing a virtual origin for the mixing region at a point upstream of the actual beginning of the mixing zone, while still utilizing the similarity solution as valid for large distances downstream. This is a good approximation as any initial velocity disturbance, such as a boundary layer, loses its effect on the shape of the flow profiles far downstream yet retains the momentum defect. Kirk (5) has suggested that the virtual origin be thirty initial momentum thicknesses upstream from the point of separation. McDonald (6) and Nash (7) found this value to produce reasonable results. Of course, near the separation point the use of the similarity velocity profile would tend to give erroneous results for most practical conditions.

<u>Developing Profiles</u> Methods of predicting the pre-asymptotic mixing region have been reported by Nash (7) and Lamb (8). These methods examine the linearized solution before the position parameter approaches zero, as it would

for large distances or zero initial boundary layer thicknesses. Lamb applied the Navier-Stokes equations along the dividing streamline to evaluate the position parameter. Once the value of the position parameter is known the local velocity profile can be identified through the pre-asymptotic solution of the linearized mixing layer equation.

In the present case, temperature profiles in the mixing region and the effects of initial temperature boundary layers are important in the complete cavity analysis. None of the above mentioned methods seemed directly applicable as no account was made of initial temperature profiles nor had any provision been made for finite velocities in the wake. Consequently a more general result had to be obtained by numerically solving the fundamental equations governing constant pressure mixing. This method may be considered more exact and informative than the approximate explicit solutions but certainly not as convenient in use. An advantage of the more general solution is that initial conditions (velocity and temperature profiles) may be studied directly whereas they had to be treated in lumped parameter form in the linearized solutions.

The solutions to the linearized equation also required a numerical evaluation and it is not clear that a numerical evaluation of the exact solution of the linearized differential equations involves less computational time than the numerical solution to the non-linear differential equation.

It is then the purpose here to establish a numerical method for the solution of the system of non-linear, partial differential equations (continuity, momentum, and energy equations) for a shear flow when the initial conditions for both streams are given. This solution should be useful in calculating the wake due to separation of any sharp trailing edged body but in the present work it is to be used in the dissipative and heat transfer models.

If the governing equations for an isobaric shear region are written in terms of a stream function they appear as,

momentum,

$$\frac{\partial u}{\partial x} = \frac{\partial}{\partial \psi}\left(\rho^2 u \epsilon_t \frac{\partial u}{\partial \psi}\right)$$

energy,

$$\frac{\partial}{\partial x}(c_p T) = \frac{\partial}{\partial \psi}\left(k \rho u \frac{\partial T}{\partial \psi}\right) + \rho u^2 \epsilon_t \left(\frac{\partial u}{\partial \psi}\right)^2$$

where by definition,

$$\rho u = \frac{\partial \psi}{\partial y} \quad ; \quad \rho v = -\frac{\partial \psi}{\partial x}$$

The continuity equation is automatically satisfied by introduction of the stream function as an independent variable.

If it is now assumed that

$$Pr_t = \frac{c_p \epsilon_t \rho}{k} = \text{CONSTANT}$$

C_p = CONSTANT

$\epsilon_t = \epsilon(x)$ ONLY

and non-dimensional variables are defined as

$$\phi = \frac{u}{u_a}, \quad \xi = \frac{x}{\delta_o}, \quad \bar{\epsilon} = \frac{\epsilon_t}{\nu}, \quad \bar{\rho} = \frac{\rho}{\rho_a}$$

$$\bar{T} = \frac{T}{T_a}, \quad \bar{\psi} = \frac{\psi}{\rho_a u_a \delta_o}, \quad Re_\delta = \frac{u_a \delta_o}{\nu}$$

where subscript "a" signifies free stream and "o" is the origin of the mixing zone then

$$\frac{\partial \phi}{\partial \xi} = \frac{\bar{\epsilon}}{Re_\delta} \frac{\partial}{\partial \bar{\psi}} \left(\bar{\rho}^2 \phi \frac{\partial \phi}{\partial \bar{\psi}} \right)$$

$$\frac{\partial \bar{T}}{\partial \xi} = \frac{\bar{\epsilon}}{Re_\delta Pr_t} \frac{\partial}{\partial \bar{\psi}} \left(\bar{\rho}^2 \phi \frac{\partial \bar{T}}{\partial \bar{\psi}} \right) + \frac{2C_a^2}{1-C_a^2} \frac{\phi}{\bar{\rho}^2} \left(\frac{\partial \phi}{\partial \bar{\psi}} \right)^2$$

For the incompressible case $Ca^2 = 0$. If the perfect gas law applies and since the pressure is constant, the equation of state may be written,

$$\bar{\rho} = \frac{1}{\bar{T}}$$

The equations are of the parabolic type and the boundary conditions are specified on the open boundary as:

(1) @ $\xi = 0$ $\quad \phi = \phi_o(\psi)$, $\bar{T} = T_o(\psi)$

(2) @ $\xi \to \infty$ $\qquad \phi = 1$, $\bar{T} = 1$

(3) @ $\xi \to -\infty$ $\qquad \phi = \phi_b$, $\bar{T} = \bar{T}_{ob}$

It can be noted that the energy equation is always coupled with the momentum equation, while the latter becomes independent from the former if density changes can be neglected (and the turbulent eddy viscosity remains unaffected by non-uniform thermal conditions).

As these are parabolic type equations, the downstream conditions are uniquely determined from known initial conditions. Values of ϕ and $\bar{T}$ then may be calculated in the positive x direction using a forward difference approximation. After the difference equations have been developed, we shall establish a stability criterion between the grid size and the parameters of the problem.

A uniform rectangular grid spacing was used as shown in the below sketch.

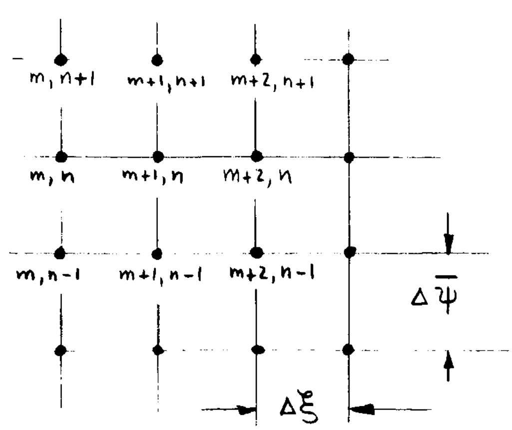

The dependent variables are calculated for the node points and are subscripted by the appropriate designation as shown.

To obtain a difference approximation for a first order derivative in ξ Taylor series expansion may be written for φ at the M+1 node in terms of its derivatives. Note that the derivation of the difference equations will be in terms of velocity but are similar for temperature in the energy equation.

$$\varphi_{m+1,n} = \varphi_{m,n} + \Delta\xi \left.\frac{\partial\varphi}{\partial\xi}\right|_{m,n} + \frac{\Delta\xi^2}{2!} \left.\frac{\partial^2\varphi}{\partial\xi^2}\right|_{m,n} + \frac{\Delta\xi^3}{3!} \left.\frac{\partial^3\varphi}{\partial\xi^3}\right|_{m,n} + \text{higher order terms}$$

Solving for the first order derivative and making $\Delta\xi$ as arbitrarily small, the maximum size of $\Delta\xi$ will be determined by stability criterion later.

$$\left.\frac{\partial\varphi}{\partial\xi}\right|_{m,n} \simeq \frac{\varphi_{m+1,n} - \varphi_{m,n}}{\Delta\xi}$$

provided that all higher order derivatives exist. The error in the approximation is of the order,

$$\xi_\epsilon \simeq \frac{\Delta\xi}{2!} \left.\frac{\partial^2\varphi}{\partial\xi^2}\right|_{m,n}$$

The same equation for the first order derivative is used for the $\bar{\psi}$ independent variable,

$$\left.\frac{\partial W}{\partial \bar{\psi}}\right|_{m,n} = \frac{W_{m,n+1} - W_{m,n}}{\Delta \bar{\psi}}$$

with an error estimate of

$$\bar{\psi}_{\epsilon} \simeq \frac{\Delta \bar{\psi}}{2!} \left.\frac{\partial^2 W}{\partial \bar{\psi}^2}\right|_{m,n}$$

If

$$W = \bar{\rho}^2 \varphi \frac{\partial \varphi}{\partial \bar{\psi}}$$

then we may write

$$\left.\frac{\partial W}{\partial \bar{\psi}}\right|_{m,n} = \frac{\bar{\rho}^2_{m,n+1} \varphi_{m,n+1} \left.\frac{\partial \varphi}{\partial \bar{\psi}}\right|_{m,n+1}}{\Delta \bar{\psi}}$$

$$- \frac{\bar{\rho}^2_{m,n} \varphi_{m,n} \left.\frac{\partial \varphi}{\partial \bar{\psi}}\right|_{m,n}}{\Delta \bar{\psi}}$$

if we now substitute for $\partial\varphi/\partial\bar{\psi}$ a difference equation and set

$$\overline{\rho^2 \varphi}_{m,n+1} = \frac{\rho^2_{m,n+1} \varphi_{m,n+1} + \rho^2_{m,n} \varphi_{m,n}}{2}$$

we obtain

$$\left.\frac{\partial W}{\partial \bar{\psi}}\right|_{m,n} = \frac{\overline{\rho^2 \varphi}_{m,n+1} \varphi_{m,n+1}}{(\Delta \bar{\psi})^2} + \frac{\overline{\rho^2 \varphi}_{m,n} \varphi_{m,n-1}}{(\Delta \bar{\psi})^2}$$

$$- \frac{(\overline{\rho^2 \varphi}_{m,n+1} + \overline{\rho^2 \varphi}_{m,n}) \varphi_{m,n}}{(\Delta \bar{\psi})^2}$$

On substitution into the momentum equation and solving for the downstream velocity term,

$$\phi_{m+1,n} = \frac{\overline{\rho^2\phi}_{m,n}\,\phi_{m,n-1} + \overline{\rho^2\phi}_{m,n+1}\,\phi_{m,n+1}}{M}$$

$$\frac{(M - \overline{\rho^2\phi}_{m,n+1} - \overline{\rho^2\phi}_{m,n})\,\phi_{m,n}}{M}$$

where the factor M is defined,

$$M = \frac{(\Delta\bar{\psi})^2\,Re_\delta}{\Delta\xi\;\bar{\epsilon}(\xi)}$$

Similarly the difference equation for $\overline{T}$ is,

$$\overline{T}_{m+1,n} = \frac{\overline{\rho^2\phi}_{m,n}\,T_{m,n} + \overline{\rho^2\phi}_{m,n+1}\,T_{m,n+1}}{E}$$

$$\frac{(E - \overline{\rho^2\phi}_{m,n+1} - \rho^2\phi_{m,n})\,\overline{T}_{m,n}}{E}$$

where E is defined

$$E = \frac{(\Delta\psi)^2\,Re_\delta\,Pr_t}{\Delta\xi\;\bar{\epsilon}(\xi)} = Pr_t\,M$$

With known values, initial conditions, or computed values of $\phi_{m,n}$ and $\overline{T}_{min}$, the downstream nodes may be calculated for given values of Re_δ and Pr_t and a known function for turbulent eddy viscosity.

Below is a sketch indicating the procedure of calculating a node from three upstream nodes using the above difference equations.

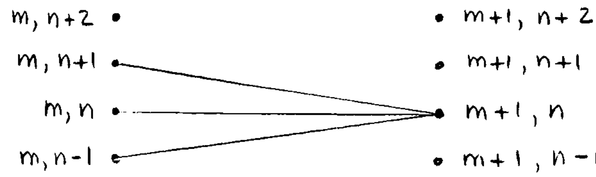

Note that for this method there is no way to calculate the outside nodes of the new column. Although the field goes to infinity in both the positive and negative $\bar{\psi}$ directions, the disturbance due to the initial difference at the origin is only effective to the edges of the shear region. Outside this region the original free stream velocities exist. At the origin, the location of the initial conditions, the disturbance edges are the boundary layer thicknesses of the two streams. As long as the field is defined outside the shear region far enough to permit the next set of nodal values to be calculated, the complete field is defined. A new set of $\bar{\psi}$ values must be inspected after every step in the ξ direction and the number of nodes increased if needed as the edges of the shear region spread. In the present analysis the outside three nodes were kept at the respective free stream values on both sides of the shear region. When the inner one of the three nodes changed by a specified tolerance, a new node was added to that side. This also allowed the outer nodal values of the new column to be set equal to the previous outer nodal values as no change could have been felt at that position. Figures 6 and 7 are an illustration of the numerical results. Note that as the solution progressed downstream, the velocity field spread and the required additional nodes were added.

Under certain conditions the solution of partial differential equations by finite difference approximations is stable and any small error (such as round-off error or small errors in the initial conditions) at some point in the calculation become smaller as the numerical procedure advances downstream. When instability exists these small errors grow and cause completely unreasonable results (from a physical point of view). A stability criterion will now be established using Karplus' electric analogue method (12). The resulting criterion will then be examined from a physical examination of the problem.

Following the Karplus Method, we arrange the difference equation as,

$$a(\phi_{m,n+1} - \phi_{m,n}) + b(\phi_{m,n-1} - \phi_{m,n})$$

$$+ c(\phi_{m+1,n} - \phi_{m,n}) + d(\phi_{m-1,n} - \phi_{m,n}) = 0$$

where the coefficient a is a positive value.

One of two conditions must be met to insure stability:

(1) Either all coefficients must be positive

or

(2) If one of the coefficients is negative, the sum of all the coefficients must be negative.

On arranging the equation for φ in the Karplus form,

$$\overline{\rho^2\varphi}_{m,n+1}(\phi_{m,n+1} - \phi_{m,n}) + \overline{\rho^2\varphi}_{m,n}(\phi_{m,n-1} - \phi_{m,n})$$

$$- M(\phi_{m+1,n} - \phi_{m,n}) = 0$$

as

$$a = \overline{\rho^2\varphi}_{m,n+1}$$

$$b = \overline{\rho^2\varphi}_{m,n}$$

$$c = -M$$

$$d = 0$$

and because C is negative (all the terms forming M are positive) the second condition must be met as there is one negative coefficient.

On adding the coefficient and applying the condition of stability

$$\overline{\rho^2\varphi}_{m,n} + \overline{\rho^2\varphi}_{m,n+1} - M < 0$$

If we examine the difference equation, we note that the coefficient of the last terms must be positive to exert a positive influence on the downstream velocity. This is the same condition as above.

Examination of φ and $\bar{\rho}$ from a physical consideration of the problem shows that the maximum values are,

$$\varphi_{max} = 1$$

$$\bar{\rho}_{max} = 1$$

therefore from the above equation

$$M > 2$$

or

$$\Delta \xi < \frac{(\Delta \bar{\psi})^2 Re_\delta}{2 \bar{\epsilon}_{max}}$$

For the energy equation a similar result was obtained with a in place of M of the momentum equation. The stability criterion then was

$$\Delta \xi < \frac{(\Delta \bar{\psi})^2 Re_\delta Pr_t}{2 \bar{\epsilon}_{max}}$$

which is a more stringent requirement for Pr_t less than one. In the present work, however, Pr_t was assumed equal to one.

Step size in the $\bar{\psi}$ direction was set by a trial and error procedure. That is a $\Delta\bar{\psi}$ size was selected and the result then compared with a previous calculation for a different size. Note that in the present method it is not necessary to assume the lateral component of velocity, v, as negligibly small. In fact it may be calculated from the continuity equation and the definition of the stream function once ϕ and $\bar{\rho}$ are known.

To proceed in the calculation, a form for the empirical eddy viscosity ratio and a value for the initial eddy viscosity must be determined. From Prandtl's mixing length theory the eddy viscosity is assumed constant over the width of the mixing region and therefore independent of the y direction (24). In the present work, as a first approximation, a linear relation in x (only) was used for the viscosity ratio although it was realized that the eddy viscosity varies across the shear layer in the pre-asymptotic region. Perhaps the more complex forms offered by either Nash (7) or Lamb (8) could be used and compared with the results obtained in this study. The immediate objective here was to obtain a reasonable yet simple model for use in the cavity analysis and not to explore all the detailed points of two-stream mixing.

The linear relation was selected as

$$\bar{\bar{\epsilon}} = a + bx$$

where

$$\bar{\bar{\epsilon}} = \bar{\epsilon}\,\frac{\nu}{\epsilon_{t_o}} = \frac{\epsilon_t}{\epsilon_{t_o}}$$

with the conditions

1) @ $x = 0$, $\bar{\bar{\epsilon}} = 1$

2) @ $x = \dfrac{-30\,n\,\delta}{(n+1)(n+2)}$, $\bar{\bar{\epsilon}} = 0$

The latter condition introduces a virtual origin which was defined by Kirk (5) for turbulent free shear layers. He postulated that

$$x_{virtual} = 30\,\theta$$

By using the definition of momentum thickness and a n power law profile for the boundary layer (24),

$$\frac{\theta}{\delta} = \frac{n}{(n+1)(n+2)}$$

we may determine the above form of $x_{virtual}$.

Consequently the following form for eddy viscosity ratio was obtained

$$\bar{\bar{\epsilon}} = 1 + \frac{(n+1)(n+2)}{30\, n} \xi$$

From velocity measurements made in the shear region of the cavity model it was estimated that the initial value for the empirical parameter would be of the order*

$$\frac{\bar{\bar{\epsilon}}}{\bar{\epsilon}} Re_\delta = \frac{\nu}{\epsilon_{t_o}} Re_\delta = 1000$$

The difference equations were programmed in Fortran II for the University of Illinois IBM 7094 digital computer. This was done in subroutine form so that the program could subsequently be used as part of a complete cavity flow and heat transfer analysis. Provisions were made to accept any initial velocity and temperature profile in a physical coordinate system and convert in the program to the ξ , $\bar{\psi}$ coordinates. Profiles could be printed, or read into the main program at any cross section in terms of an intrinsic

---

*Using the virtual origin equation of Kirk and data presented in "Basic Research Investigation of Flow Mechanisms and Heat Transfer in Separated Flows," Semi-Annual Status Report SR-13 for NASA NsG 13-59, December 20, 1966, a check could be made on this estimate. It was found that the value at x = 0 and the linear form adopted here were in good agreement with results obtained from hot wire measurements in the shear zone.

coordinate system. These profiles were converted to the physical system of coordinates by making a momentum and continuity balance at the desired cross section. In the present case of the cavity, this was done at the reattachment location so that the "j" and "d" streamlines could be located.

In Figure 5, φ_j, the velocity along the streamline emanating from the origin, is compared for the present analysis with a zero boundary layer thickness at the origin to the corresponding one for the fully developed profiles of reference 2. The two methods agree quite well showing only a maximum of a 3 per cent difference in the range calculated. This indicates that the difference equations at least calculate a velocity field in the fully developed region that matches an accepted asymptotic solution.

The net mechanical energy transfer in the shear region may now be calculated from

$$\bar{E}_T = \frac{E_T}{\frac{1}{2}\rho_a u_a^3 \ell_m} = I_4(\omega)$$

where

$$I_4(\omega) = \int_{-\infty}^{\omega} \frac{\rho}{\rho_a}\varphi(\varphi^2 - \varphi_b^2)\, d\omega$$

This integral was evaluated numerically using the velocity distribution at the point of reattachment from the jet mixing analysis.

2. The Recompression Zone--Energy dissipation in reattachment regions has not been studied in great detail for free turbulent shear mixing. It appears that the sharp edge at reattachment of a circular cavity reduces the dissipation of reattachment to a negligible value (1).

3. The Cavity Wall Boundary Layer--Energy dissipation along the cavity wall was calculated by considering the wall as a flat plate subject to an "external" incompressible shear flow. The initial velocity profile was assumed to be that part of the mixing velocity profile at reattachment which was below the "d" streamline. Dissipation is determined by assuming that the external shear flow retains its profile outside of the boundary layer and that the wall velocity distribution follows a n-power law profile (1).

Application of the momentum integral method along the cavity wall resulted in an ordinary differential equation.

$$d\left(\frac{\delta}{\ell_m}\right)\left[\varphi_\delta^2 \frac{2}{n+2} - \varphi_\delta \varphi_\delta \frac{1}{n+1}\right]$$

$$+ d\varphi_\delta \frac{\delta}{\ell_m} \frac{n}{n+1}\left[\varphi_b - \varphi_\delta \frac{2(n+1)}{n+2}\right]$$

$$= 0.0225\,(\varphi_\delta)^{\frac{2n}{n+1}} \left(\frac{\delta}{\ell_m}\right)^{\frac{-2}{n+1}} (Re_m)^{\frac{-2}{n+1}}\, d\left(\frac{X}{\ell_m}\right)$$

This was solved numerically using the numerically calculated mixing velocity profile at reattachment with the initial conditions,

$$@\ \frac{x}{\ell_m} = 0\ ,\ \frac{\delta}{\ell_m} = 0\ ,\ \varphi_\delta = \phi\,(\eta_d)$$

and yielding the dissipation in the wall boundary layer as,

$$\overline{E}_{D_{BL}} = \frac{E_{D_{BL}}}{\frac{1}{2}\rho_a u_a^3 \ell_m} = I_4(\omega_d) - I_4(\omega_\delta)$$

$$+ \frac{\delta}{\ell_m}\varphi_\delta^3 \frac{n}{n+1}\left[\left(\frac{\varphi_b}{\varphi_\delta}\right)^2 - \frac{n+1}{n+3}\right]$$

where the integrals, I_4, are as previously defined.

4. <u>The Cavity Core Region</u>--The dissipation in the core region was set equal to zero as the cavity shape considered leads to a core flow pattern resembling a solid body rotation. The mass which was bled into the cavity was assumed to enter with zero velocity at the center of the core region. As the velocity at the center of the core of a solid rotating body is also zero, there is no relative velocity and therefore no mechanical energy dissipation to be considered due to the mass bleed.

The energy balance has now been reduced to two terms. In short, the net mechanical energy transferred by the mixing process is equal to the energy dissipation along the cavity wall.

$$\frac{E_T}{\frac{1}{2}\rho_a u_a^3 \ell_m} = \frac{E_{D_{BL}}}{\frac{1}{2}\rho_a u_a^3 \ell_m}$$

The unknown wake velocity, ϕ_b, the peak velocity at the cavity wall at the separation point, serves as the cavity reference velocity. It is considered as the local peak velocity in secondary stream of the two-stream analysis and is also representative of the dissipation along the wall. This reference velocity thus characterizes the velocity field throughout the wake region and represents the secondary stream velocity in the jet mixing analysis. It was used as the independent variable in satisfying the mechanical energy balance. Figure 8 is an example of the results of the matching technqiue whereby ϕ_b is assumed and the two mechanical energy terms are calculated.

The calculation procedure for the balance was achieved as follows for a given cavity geometry and free stream conditions:

(1) assume a value for ϕ_b

(2) calculate the mixing solution by using for initial conditions,

a. the free stream velocity profile at the point of separation. This may be a calculated or an experimentally measured profile.

b. an n-power law velocity profile representation for the secondary stream based on ϕ_b and ℓ_w at the point of confluence.

c. a secondary stream temperature profile at the point of confluence (described in the subsection on cavity wall heat transfer).

(3) calculate the dissipation along the cavity wall as that of a boundary layer in a shear flow on a flat plate, $\bar{E}_{D_{BL}}$. The initial shear velocity profile is the terminal velocity profile of the mixing solution at the point of reattachment.

(4) calculate net energy transferred, $\bar{E}_T$.

(5) compare $\bar{E}_T$ and $\bar{E}_{D_{BL}}$. If the energies are not balanced, change the secondary initial velocity and temperature profiles based on the new ϕ_b. Return to the first step in the procedure and continue until a balance is achieved. Figure 8 is a graphical example of the numerical iteration performed by the digital computer.

After the balance has been achieved, complete information is available on the velocity field of the cavity. These results are then used in a thermodynamic balance to calculate the convective energy transfers.

In Figure 3, the cavity reference velocity, ϕ_b, is shown as a function of the ratio of cavity wall length to mixing length with data due to Golik. The curve was calculated with the present analysis using a calculated and experimentally compared n-power law initial velocity profile of the primary stream based on the cavity leading plate length reported by Golik (see Figure 10). The data show general agreement in the trend and give credulence to the present method of analysis. There cannot be a complete comparison as Golik did not specifically report the initial boundary layer thickness for his circular cavity. A boundary layer trip was used by him to insure a turbulent boundary layer. Therefore, it is reasonable to expect that his experimental boundary layer thickness would be larger than that calculated from an n-power law. As shown in reference 1 for the similarity analysis, φ_t decreases with increasing initial boundary layer thickness. This would seem to indicate the reason for the general shift in the data as compared to the analysis.

B. Heat Transfer Model

As was the case for the dissipative model, there is no published comprehensive analysis of heat transfer in a cavity with mass bleed and non-isothermal walls. Korst (1) and Miles (4) have developed a simplified analytical model for heat transfer to and across cavities on the basis of finite wake velocities resulting from the dissipative flow model developed by Golik (3). A summary of some of the experimental work published (14-18) is given below followed by a presentation of the heat transfer model using a systems analysis similar to the method used for the dissipative model.

Larson (14) conducted an experimental program with an axisymmetric model. In the laminar regime the results apparently agreed well with the laminar mixing layer analysis of Chapman (15). However, he found large disagreement with Chapman's predictions for the turbulent regime. This was evidently due to the assumption that the cavity bulk temperature was equal to the wall temperature. The bulk temperature was measured for the turbulent case and found in fact not to be equal to the wall temperature. The average measured heat transfer coefficients were proportional to the length Reynolds number raised to the -0.5 power for laminar flow and the -0.4 power for turbulent flow.

Charwat (16) reported local heat transfer for rectangular cavities. These experiments tended to confirm Larson's results with respect to the Reynolds number. The report described the complex multiple vortices of a rectangular cavity. Also it was noted, by experiment, that the initial boundary layer temperature history does bear some influence on the heat transfer in the cavity.

Fox (17) made experimental measurements for rectangular cavities with length ratios, e/h ranging from $\frac{1}{4}$ to $1\frac{3}{4}$.

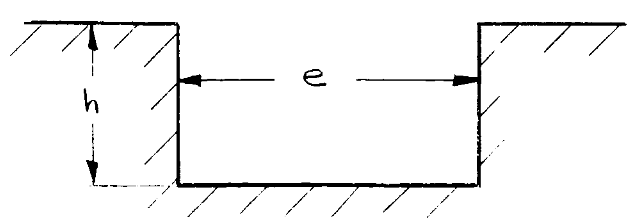

He found that the heat transfer coefficients were proportional to the length Reynolds raised to the -0.2 power for turbulent boundary layers. Seban (18) using the same facilities as Fox reported measurements for the rectangular cavity with length ratios over the range of 2 to 5.

S. M. Bogdonoff (11) at Princeton University's Gas Dynamics Laboratory has conducted tests in the hypersonic regime with laminar flow over axisymmetric cavities with mass bleed used for cooling. The article contained no analysis or complete data but claimed that the heat transfer rate to the body could be reduced to zero with the proper amount of bleed (depending on the cavity shape). Work was done investigating the influence of the reattachment shoulder geometry not only on the cavity heat transfer but also on that heat transfer occurring on the surface downstream of the cavity.

Miles in his analysis (4) assumes that the heat transferred from the constant temperature cavity wall into the thermal boundary layer is released as a line source at the point of confluence (separation point of the external stream, S in figure 4), the point of origin of the jet mixing. To make the point of the source coincide with the origin of the jet mixing it was necessary to assume zero initial boundary layer thickness in the primary and secondary streams of the mixing process. Mass bleed into the cavity was not considered.

Energy of the line source was considered diffused in the mixing region and the temperature profile due to the source was obtained from a solution of the energy equation which assumed similar solutions. The temperature profile thus obtained was superposed to the temperature profile established by jet mixing to obtain the total temperature profile. The local wall heat transfer was determined from Reynolds analogy for a flat plate using the velocity profiles from Golik's dissipative model. Total heat transfer was calculated from a numerical integration of the local heat flux (1).

The present analysis was made for non-isothermal cavity walls with mass bleed in the cavity core region. The dissipative model described in the previous section was used to establish the finite wake velocity profiles. By using the numerical solution to the jet mixing region it is now possible to account for finite boundary layers in either stream at the point of separation. It is also not necessary to assume a similar solution for the temperature profiles in the shear zone as temperatures were also calculated through the mixing region in the numerical solution.

A systems energy balance was made for the cavity using the same assumptions of flow conditions and geometry that were used for the dissipative model. The system boundaries for the heat transfer model are shown in figure 4 with the individual terms identified. These boundaries are the same as those of the dissipative model. All heat added to the system was considered positive as is the usual thermodynamic convention.

The energy balance yields an equation of the form,

$$Q_w + Q_d + Q_m + c_p T_{os} G_s = W_m + \int_{y_d}^{y_j} T_o c_p \rho u \, dy$$

The energy components are:

(1) Q_W, the heat transfer from the cavity wall into the wall thermal boundary layer.

(2) Q_d, the heat diffused to the free stream (outside of streamline "j") from the total Q_W released at the point of confluence due to the wall boundary layer.

(3) Q_m, the heat transferred across the streamline "j" in the mixing region.

(4) $C_p T_{os} G_s$, the energy added to the system due to mass bleed at a temperature T_{os}.

(5) W_m, the shear work transferred across the streamline "j" in the mixing region.

(6) The energy leaving between the "j" and "d" streamlines due to mass addition.

The energy terms in the mixing region may be written in terms of temperature as,

$$W_m - Q_m = \int_{y_j}^{\infty} c_p \left(T_o - T_{oa} \right) dy$$

also noting that the integral may be rewritten,

$$\int_{y_d}^{y_j} \rho u c_p T_o \, dy = \int_{y_d}^{y_j} \rho u \, c_p \left(T_o - T_{oa} \right) dy + \int_{y_d}^{y_j} \rho u \, c_p \, T_{oa} \, dy$$

and that on the basis of conservation of mass,

$$G_s = \int_{y_d}^{y_j} \rho u \, dy$$

one then may solve for the wall heat transfer term and obtain,

$$Q_W = \int_{y_d}^{\infty} c_p \rho u \left(T_o - T_{oa} \right) dy - c_p G_s \left(T_{os} - T_{oa} \right)$$

which may be normalized as,

$$\overline{Q}_W = \frac{Q_W}{\rho_a u_a c_p \ell_m T_{oa}} = \int_{\omega_d}^{\infty} \frac{\rho}{\rho_a} \phi \left(\Lambda - 1 \right) d\omega - \overline{G}_s \left(\frac{T_{os}}{T_{oa}} - 1 \right)$$

where $\omega = y/\delta_o$ is the transverse dimension in the mixing region normalized by the initial boundary layer thickness of the primary or free stream. This is compatible with the variable defined in the two-stream numerical solution.

The equation is now in a form similar to the mechanical energy equation. That is the wall heat transfer (mechanical energy wall dissipation) is equal to the net heat transferred from the cavity (net mechanical energy transferred) minus the efflux of energy due to mass bleed (efflux of mechanical energy). Each term will be analytically determined in the following.

1. Wall Heat Transfer--In considering the wall heat transfer, it is apparent that the initial conditions at the point of reattachment of the jet mixing region are non-uniform in both velocity and temperature. This situation is due to the fact that these velocity and temperature profiles are identical with the lower (*i.e.*, $y < y_d$) portion of the mixing profiles at reattachment, which is the beginning of the cavity wall flow regime. The velocity profile was taken into account in determining the wall mechanical energy dissipation and was also used in a similar manner in determining the wall heat transfer. The wall heat transfer with an arbitrary temperature distribution was assumed similar to heat transfer from a flat plate with the same temperature distribution.

A survey was made of work published on flat plate heat transfer to an incompressible boundary layer but the case of interest here was not reported. It was felt that as a first approximation a reliable method of calculating heat transfer from a non-isothermal plate would be selected from the literature and that this method would be modified to account for the non-uniform initial conditions in a manner similar to the wall dissipation. The resultant equation, of course, would be subject to experimental verification.

There are several general survey articles on flat plate heat transfer of which Nickerson (19) and Kisten (20) are examples. The general boundary layer equations were developed and a discussion of several methods of solution and their limitations were made including a presentation of equations for variable wall temperature.

Spalding (21) presents an exact solution of the partial differential equations for the case of a step discontinuity in wall temperature. The solution depends on his unique single formula for the law of the wall (22). It is a complex solution when compared to the semi-empirical results of other investigators and not easy to use in a superposition technique to determine local wall flux for non-uniform wall temperatures.

Hartnett et all (23) survey the methods specifically derived for non-uniform temperatures and conclude that the analyses are difficult to apply for completely arbitrary wall temperature distribution. The authors simplify the resultant equations and present an approximate form that may be readily used on engineering problems. Several examples were worked out.

Reynolds (13) at about the same time as Hartnett published his thesis on a semi-empirical method of treating non-uniform wall temperatures. The method is easy to use, his description is complete, and an experiment was designed and performed verifying his results. These equations for local heat flux were modified and used to calculate local and total heat flux from the cavity wall for non-isothermal walls. Following is a brief description of the analysis:

The investigation was done in three parts:

(1) flat plate with constant temperatures

An approximation of the von Karman analogy with the Schultz-Grunow friction formula for use in the local Reynolds Number range of 10^5 to 10^7 was selected after a review of the constant temperature case.

$$St_T = 0.0296 \, Re_x^{-1/5} \left(\frac{T_W}{T_{ob}} \right)^{-2/5} (Pr)^{-2/5}$$

The temperature ratio is a correction term which allows the fluid properties to be calculated at free stream temperature. This correction is only important if the wall temperature is considerably different than the free stream temperature. Note that in the present case the free stream velocity in the Reynolds number will vary along the length of a plate representing the cavity wall due to the initial shear flow profile.

(2) flat plate with a step temperature change

An approximate solution was obtained for heat transfer for a step change

$$\frac{St(x)}{St_T} = \left[1 - \left(\frac{\ell}{x} \right)^{9/10} \right]^{-1/9}$$

where ℓ is the location of the step from the leading edge of the plate. This was compared to solutions available in the literature and found reasonable. It also agreed well with data obtained by Reynolds.

(3) flat plate with variable wall temperature

For the variable temperature case, one may now superimpose an infinite number of small steps using the step change result. This resulted in the following expression

$$q_b(x) = \int_{\xi=0}^{x} h(\xi; x) \, dT_w(\xi)$$

where

$$h(\xi; x) = \rho u c_p St_T \left[1 - \left(\frac{\xi}{x} \right)^{9/10} \right]^{-1/9}$$

The above integral is not the ordinary Riemann or area type of integral, but rather a Stieltjes integral as the prescribed wall temperature can have discontinuities so that the derivatives are undefined at these points.

To enable evaluation of the integral, it may be expressed in terms of a Riemann integral and a series which accounts for the finite discontinuities.

$$\int_0^x h(\xi;x)\,dT_w(\xi) = \int_0^x h(\xi;x)\,\frac{dT_w(\xi)}{d\xi}\,d\xi + \sum_{m=1}^{N} h(\ell_n;x)\left[T_w(\ell_n^+) - T_w(\ell_n^-)\right]$$

where $T_w(\ell_n^+) - T_w(\ell_n^-)$ is the temperature change across the n^{th} discontinuity located at ℓ_n.

On examining the equation for $h(\xi;x)$, it is apparent that for all but the simplest cases the integral cannot be solved in closed form and that each case would require its own particular numerical integration to determine the local heat transfer rate. The numerical result would then have to be integrated again to obtain the total heat transferred from the cavity wall.

Following Hartnett (23) and others, Reynolds proposed representing the variable wall temperature by a finite number of ramps. The results for a general ramp may be obtained from the above equation.

A general temperature profile for a ramp starting at any location, a, on the plate, is

$$\Delta T = 0 \quad , \quad x < a$$

$$\Delta T = m(x-a) \, , \quad x > a$$

then the heat rate is

$$q(x) = \rho u c_p St_T m \int_{\xi=a}^{x} \left[1 - \left(\frac{\xi}{x}\right)^{9/10}\right]^{-1/9} d\xi$$

transforming the variable by setting

$$z = 1 - \left(\frac{\xi}{x}\right)^{9/10}$$

the following is obtained

$$q(x) = \frac{10}{9} \rho u c_p St_T m_x \int_0^{1-\left(\frac{a}{x}\right)^{9/10}} z^{-1/9} (1-z)^{1/9} dz$$

where the integral may be recognized as the Incomplete Beta Function. This function has been tabulated for various parametric values of exponents. The function needed at present is plotted in figure 10 with a table of the values used for the plot.

Any variable temperature distribution may be approximated by

$$\frac{T_w(x) - T_o}{T_o} = \sum_{m-1}^{N} \left(\frac{x}{\ell_m} - A_n \right) M_n + \sum_{j=1}^{J} B_j$$

where A_n = location of n^{th} ramp divided by a reference length

M_n = slope of n^{th} ramp normalized with a reference length and the reference free stream temperature.

B_j = j^{th} step change in temperature normalized by reference free stream temperature.

Note that the ramps and steps are only to be effective from the points of origin downstream. The heat rate may be written

$$\frac{q_t(x)}{T_o} = \frac{10}{9} \rho u c_p St_T(x) \left\{ \frac{x}{\ell_{ref.}} \sum_{m=1}^{N} M_n Br_n (8/9, 10/9) \right.$$

$$\left. + \sum_{j=1}^{J} B_j \left[1 - \left(L_j \frac{\ell_{ref}}{x} \right)^{9/10} \right]^{-1/9} \right\}$$

where

$$Br_n(a, b) = \int_0^{r_n} z^{a-1} (1 - z)^{b-1} \, dz$$

$$r_n = 1 - \left(A_n \frac{\ell_{ref}}{x} \right)^{9/10} \qquad 0 < r \leq 1$$

L_j = location of the j^{th} step divided by a reference length.

These equations were modified for the non-uniform conditions existing at the beginning of the cavity wall at cavity reattachment and integrated over the length of the cavity wall to obtain the total heat transferred to the wall thermal boundary layer, $\overline{\Theta}_w$.

In the same sense as the dissipation analysis of the wall boundary layer provided a secondary stream boundary layer profile forming the initial velocity distribution for the two-stream mixing analysis, so does now the heat transfer calculation provide the initial temperature profile for the secondary stream. The temperature profile should thus be calculable along the wall, especially at the end of the wall. As was pointed out in reference (13), the profile will be dependent on the wall temperature history i.e., the final profile will be dependent on how the temperature varies along the length of the wall.

Reynolds presents no estimate of local temperature profiles on a flat plate for arbitrary wall temperature and in a literature search no satisfactory method was found of predicting the shape of the temperature boundary layer for this general case. Therefore, as a first approximation, in the present analysis it was assumed that the Turbulent Prandtl Number was one and that the temperature boundary layer obeyed a power law similar to the velocity boundary layer,

$$\frac{T_w - T}{T_w - T_\delta} = \left(\frac{y}{\delta}\right)^{1/n}$$

Outside the boundary layer, the initial temperature profile from the mixing solution was retained.*

Reynolds (13) shows experimentally that for uniform initial conditions the power law representation is a good approximation for constant wall temperature and for a finite number of step changes wall temperature except in the immediate vicinity of the step. For completely arbitrary wall temperature, this is a weak approximation. Because of this limitation data to confirm the analytical results were taken only for constant wall temperature and step changes.

The equation for local temperature ratio is now written,

$$\frac{\Delta T(x)}{T_{ob}} = \frac{T_w - T_\delta}{T_{ob}} = \sum_{n=1}^{N} \left(\frac{x}{\ell_m} - A_n \right) M_n + \sum_{j=1}^{J} B_j$$

where T_δ is the temperature at the edge of the boundary layer and now A_n and B_n must also take into account the initial variable temperature profile effect at the edge of the boundary layer when approximating $\Delta T(x)$ by the ramps and steps. This means that the local temperature profile must also be known to determine $\Delta T(x)$. For the limited cases here, constant temperature and step changes, the above

*While apparently reasonable for cases where friction and thermal boundary layer are of nearly the same thickness, this concept should be re-examined for much more generalized cases such as produced by step changes in wall temperature. Indeed, neglect of this point results in discontinuities for local heat transfer coefficients near step changes in wall temperature (e.g., see figures 19, 20, and 21).

power law was used. Note that the ramps and steps are effective only from the starting points and downstream.

The local heat flux was written,

$$\frac{q(x)}{T_{ob}} = c_p \rho_b u_b St_T(x) \left\{ \frac{10}{9} \frac{x}{\ell_m} \sum_{n=1}^{N} M_n Er_n(8/9, 10/9) + \sum_{j=1}^{J} B_j \left[1 - \left(L_j \frac{\ell_m}{x} \right)^{9/10} \right]^{-1/9} \right\}$$

where mixing length is the reference length in A_n and M_n and the average cavity bulk temperature is the reference temperature in B_j and M_n. One may then define an Average Stanton Number using an average wall temperature as,

$$\overline{St}_w = \frac{Q_w}{\ell_w \rho_L u_L c_p (\bar{T}_w - T_{ob})}$$

Total wall heat transfer is the integral of the local flux over the plate length which is written

$$Q_w = \ell_m \int_0^{\ell_w/\ell_m} q \, d\left(\frac{x}{\ell_m}\right)$$

Average wall temperature term for the Stanton Number was defined,

$$\frac{\bar{T}_w - T_{ob}}{T_{ob}} = \frac{\ell_m}{\ell_w} \int_0^{\ell_w/\ell_m} \left[\frac{\Delta T(x)}{T_{ob}} - \frac{T_{ob} - T_s}{T_{ob}} \right] d\left(\frac{x}{\ell_m}\right)$$

The second half of the integral is evaluated from the known initial temperature distribution and the local power law profile.

On substitution for the local temperature and completion of the integration, the first part of the integral may be written

$$\int_0^{\ell_w/\ell_m} \frac{\Delta T(x)}{T_{ob}} = \sum_{n=1}^{N} \left\{ \frac{1}{2}\left(\frac{\ell_w}{\ell_m}\right)^2 - A_n \frac{\ell_w}{\ell_m} + \frac{1}{2} A_n^2 \right\} M_n$$

$$+ \sum_{j=1}^{J} \left\{ \frac{\ell_w}{\ell_m} - L_j \right\} B_j$$

As the local velocity at the edge of the boundary layer ϕ_δ , is only available numerically, neither term in the equation for the local flux may be integrated in closed form. Therefore, the total heat flux was determined by a numerical integration of the two finite series.

The final equation for the Average Stanton Number is then,

$$\overline{St}_w = K \left\{ \frac{10}{9} \int_0^{\ell_w/\ell_m} \left(\frac{x}{\ell_m}\right)^{4/5} \phi_\delta^{4/5} \sum M_n Br_n \, d\left(\frac{x}{\ell_m}\right) \right.$$

$$+ \int_0^{\ell_w/\ell_m} \left(\frac{x}{\ell_m}\right)^{-1/5} \phi_\delta^{4/5} \sum B_j \left[1 - \left(L_j \frac{\ell_m}{x} \right)^{9/10} \right]^{-1/9} d\left(\frac{x}{\ell_m}\right)$$

where

$$K = \frac{0.0296 \left(\frac{\bar{T}_w}{T_{ob}} \right)^{-2/5} Pr^{-2/5} \; Re_m^{-1/5}}{\phi_b \frac{\ell_w}{\ell_m} \left(\frac{\bar{T}_w}{T_{ob}} - 1 \right)}$$

This equation was programmed for numerical integration on the IBM 7094 digital computer for any given wall temperature distribution, initial conditions from the mixing solution, and wall length ratio, ℓ_w/ℓ_m.

2. Net Heat Transfer in Mixing Region--A major difference between the present solution and the solution of Korst (1) and Miles is in the manner the heat transferred from the cavity wall into the thermal boundary layer is represented at the confluence point for diffusion into the mixing zone. A brief review of the later method is given below followed by an explanation of the present solution.

The earlier study assumed that the temperature field of the jet mixing region could be superimposed to a temperature field due to the diffusion of the wall boundary layer thermo energy at the point of confluence. It was assumed that the diffused temperature field could be represented by a similarity profile in addition to the similarity velocity profiles of the mixing region. There was, therefore, no direct way to account for initial boundary layer thickness in either the velocity or temperature solution in the mixing region. Indeed, it was not even attempted to account for the initial distribution of the temperature field in a way corresponding to the equivalent bleed concept for velocity profiles.

To obtain a more generally useful solution of the mixing region a numerical solution to the momentum and energy equation was made including the effects of initial temperature and velocity boundary layers. This has been described in the previous section. The heat transferred into the wall boundary layer will be carried into the mixing solution, by a temperature profile at the end of the wall (beginning of the mixing region) instead of the line source representation of Miles and Korst. An integral of the enthalpy distribution at that point should, therefore, be equivalent to the total heat transferred from the wall. As was discussed in the section on wall heat transfer, a method of determining the end temperature profile is, in general, not available for an arbitrary wall temperature distribution. This limits the reliable range of application of the solution at the present time to those cases where the thermo boundary layer temperature profile is calculable.

The integral representing the net heat transfer may be rewritten in terms of integrals that were defined for the similarity profiles (1). Of course, these integrals must be evaluated for the profiles obtained with the present jet mixing numerical solution.

$$\int_{\omega_d}^{\infty} \rho/\rho_a \, \phi \, (\Lambda - 1) \, d\omega = I_3(\omega_{Ra}) - I_3(\omega_d) - \left[I_1(\omega_{Ra}) - I_1(\omega_d) \right]$$

where the integrals are defined as

$$I_3(\omega) = \frac{\rho_b}{\rho_a} \, \phi_b \, \frac{T_{ob}}{T_{oa}} \, \omega_{Rb} + \int_{\omega_{Rb}}^{\omega} \frac{\rho}{\rho_a} \Lambda \phi \, d\omega$$

$$I_1(\omega) = \frac{\rho_b}{\rho_a} \, \phi_b \, \omega_{Rb} + \int_{\omega_{Rb}}^{\omega} \frac{\rho}{\rho_a} \, \phi \, d\omega$$

The unknown wake bulk temperature T_{ob} serves as the cavity reference temperature as the wake velocity, ϕ_b, did for the dissipative model. It is the secondary stream temperature outside the shear region in the two-stream mixing analysis which is also used in the heat transfer analysis along the cavity wall. This reference temperature thus characterizes the temperature field of the wake region. It was used as the independent variable in performing the thermal energy balance.

The calculation procedure for the thermodynamic balance was made as follows for a given cavity geometry and free stream conditions:

(1) assume a T_{ob}/T_{oa} value

(2) calculate the temperature field in the mixing region and determine the net heat transfer across the mixing region

(3) calculate the total wall heat transfer

(4) check the balance of the thermal energy equation for given mass bleed conditions. If the terms do not balance, return to step (1) and re-assume a new value of T_{ob}/T_{oa}.

After the balance has been accomplished, the temperature field for the cavity becomes known as well as the velocity field, which had been calculated before with the help of the dissipative model.

III. EXPERIMENT

A. Experimental Objectives

The theory developed for mass addition at a given temperature to a circular cavity with an arbitrary wall temperature distribution should be evaluated experimentally to determine if the underlying assumptions are reasonable and the analytical results useful as engineering design information. The results for the experimental model for the limiting cases considered provide a basis for evaluating the complete cavity heat transfer and dissipative model.

Design of the experiment should be versatile enough to extend the range of the experimental data as more recent information is added to the theoretical model as well as provide information useful to the present analysis. It should also be made flexible enough for use in further studies that might be suggested by the present work.

The object, therefore, was to design an experiment that most nearly meets the assumption of the present analysis and anticipated extensions to the analysis.

B. Experimental Apparatus

1. Model--A circular cavity 7 1/2 inches in diameter with a 9 15/16 inch opening was fabricated from lucite plastic and completely encased in fiberglass insulation one inch thick. The cavity was 14 3/8 inches wide and had lucite leading and trailing plates. A sketch is shown in figure 10 of the cavity

mounted at the outlet of the free-jet wind tunnel used in the experiment.

Lucite was used as the construction material because it is an excellent thermo and electrical insulator. These characteristics were necessary in order to keep the heat loss to a minimum and to provide electrical insulation between the heater strips that were mounted along the cavity wall to simulate wall heat transfer. The added fiberglass wrap insured low thermo losses from the heated cavity wall and from the end walls.

Driver-Harris Company 245 alloy Nichrome, one inch wide and 0.001 inches thick, ribbon was used to construct the heaters for the wall heat transfer. The heaters completely spanned the width of the cavity and the power leads were led out through the two side walls. The lead opening was calked to insure no air leakage. Duco cement was used to fasten the heaters to the wall and gave an excellent smooth bond after an initial curing period. The cement and the lucite walls limited the wall temperature less than 200° F.

Thirty-two strips were mounted along the wall with a 1/32 inch spacing between strips. This arrangement was thought to give a reasonable approximation to any arbitrary temperature. Each heater was individually manually controlled using a control shown schematically in figure 12.

Strip temperature was controlled by adjusting the rheostat shown in the schematic and monitoring the temperature on a read-out device. The adjustments continued from heater 1 through heater 32 until the desired temperatures were reached within a tolerance of $1/4^{\circ}$ F on the potentiometer. This is well within the manufacturer's tolerance on the thermocouple wire. All heaters were powered in a parallel circuit from a 120 volt to 5 volt heavy duty transformer as shown. Average heater resistance was on the order of 0.55 ohms per foot.

Copper-constantan thermocouples of 30 gage wire were mounted under the center of each strip to measure and monitor the strip temperature. Figure 11 shows a sketch of a thermocouple mounted in the lucite wall. The wires were extended two inches along the heater strip to reduce the measurement error due to heat conduction to a negligible value (30). Openings in the wall were sealed with Duco cement which was also used to hold the thermocouples in place.

Thermocouples were also mounted in various places in the wall to measure gradients between strip centers and across the cavity from one side wall to the other. At the test location, the center of the cavity wall, the gradients were within the tolerance of the thermocouple wire for a five degree difference in adjacent strip center temperatures.

The leading plate to the cavity had two purposes: firstly, to establish the flow entering the cavity in a turbulent boundary layer, and secondly, to eliminate the effects of the nozzle boundary layer of the blower. As shown in figure 10, the tunnel boundary layer is scooped under the plate. Boundary layer thickness on the leading plate was 0.31 inches at the cavity entrance. This value was based on a velocity traverse with a total pressure probe and when plotted is a representative turbulent boundary layer.

The trailing plate was used to lead off the flow that passes over the cavity. It will be interesting at a later time to install temperature measuring devices along this plate to measure the effect of changes in the cavity on heat transfer to the trailing plate.

Both edges of the cavity, at separation and reattachment, were made sharp and blended into the cavity wall. This was done to make a distinct location of separation and reattachment.

Mixing length of 9 15/16 inches corresponds to a Mixing Reynolds number of 4.8×10^5 and the cavity had a ratio of cavity wall length to mixing length of 3.35.

2. Equipment--A low speed free-jet wind tunnel located in the Mechanical Engineering Laboratory was used in this experiment. A backward curved centrifugal blower with a capacity of 1000 C F M at 7.5 inches of water or 15,500 C F M at atmospheric pressure was discharged through a diffuser into a three feet by four feet settling chamber. The chamber had two 10 x 14 mesh screens across the chamber at approximately the center which dampened any upstream disturbances and reduced the turbulence level. Downstream of the settling chamber was a nozzle with a 15 x 20 inch exit area discharging into the atmosphere. The exit velocity was approximately 100 fps, depending on the atmospheric conditions, and uniform within 0.5 per cent excluding the 0.3 inch wall boundary layer. Figure 10 indicates the

relative position of the nozzle and the cavity.

The following measurements were recorded:

a. Free Stream Velocity with a 0.049 inch diameter total pressure probe. Readings were made on a 3-inch Merriam inclined manometer, which could be read to the nearest 0.01 inch of water. The probe was mounted approximately ten inches above the cavity opening and centered with respect to the blower exhaust nozzle.

b. Free Stream Temperature with a copper-constantan thermocouple referenced to an ice bath. The thermocouple was mounted on the leading edge of the flat plate upstream of the cavity.

c. Bleed Temperature with two copper-constantan thermocouples referenced to an ice bath. The thermocouples were mounted in the couplings just before the air entering into either side of the cavity.

d. Bleed Mass Flow Rate with a Fisher and Porter Rotameter number J10-1569 with a BSX - 62 - A float and B - 6A - 25 - A tube. This meter was compared with an A.S.M.E. standard orifice meter, and the two meters were found to be within three per cent in the range of the data.

e. Cavity Temperature with four copper-constantan thermocouples in series referenced to the free stream temperature. The free stream junctions were mounted in the same location as the thermocouple measuring free stream temperature. The four couples were mounted in the cavity on a radius and at an interval that would give a meaningful average temperature. It was assumed that the core flow was solid body rotation and using this velocity profile the mass flow rate distribution along the radius of the cavity was determined. The radius was divided into four equal total mass segments and thermocouples were mounted at the mass flow center of each segment.

f. Atmospheric Pressure with a standard barometer mounted in the Mechanical Engineering Laboratory.

g. Current Flow to the heaters with a Weston meter which could be read to the nearest 0.05 of an ampere.

h. Heater Temperature with individual copper-constantan thermocouples to each of 32 heaters.

All temperature measurements were read on a Leeds and Northrup portable potentiometer which could be read to the nearest 0.001 of a millivolt. This is the nearest 1/22 of a degree for copper-constantan thermocouples and much closer than the thermocouple guaranteed tolerance of 3/4 of a degree. The millivolt readings were converted to temperature using Leed and Northrup's 31031 Standard Conversion Tables. All thermocouples were constructed from 30 gage nylon insulated wire. The wire was calibrated by the manufacturer, Thermo Electric Co., Inc., and an accuracy of $\pm 3/4^{\circ}$ F from 75° F to 200° F was guaranteed.

C. Experimental Procedure

The test was conducted in the following fashion:

a. Start the wind tunnel and record free stream conditions and barometric pressure.

b. Adjust the cavity bleed rate to the predetermined value.

c. Turn on heater to mass bleed. This was not precisely controlled at a given temperature but set with a Variac transformer. Settings were made to cover a particular range of bleed temperatures.

d. Turn on power to heater strips and preset heater controls based on past experience for the desired temperature distribution.

e. Allow approximately 30 minutes to pass and then make any fine adjustments needed for the bleed rate.

f. Change each individual heater controls until the desired temperature distribution is set. This usually requires on the order of 30 minutes and a great deal of patience.

g. Record power to each heater, cavity temperature, and wall temperature distribution.

IV. DISCUSSION OF RESULTS

In contrast to earlier investigations which proposed and attempted to verify individual and supposedly mutually independent components, as well as their integration into the over-all cavity flow model, this study has been conducted in anticipation of strong interactions between flow regions and different dissipative and convective mechanisms.

In particular, the jet mixing problem had to be linked together with the initial velocity and temperature distributions near the point of confluence which required the study of developing non-similar profiles. The problem of dealing with the effective eddy viscosity in an analytical model, although important, has been coped with in a cursory form only and no direct evidence has been sought or obtained in the course of this study.

However, the analytical method, as presented, can yield numerical solutions in a form which do not require full specification of the viscosity law, and any information going beyond such preliminary formulations as proposed in section II and used for all analytical results could easily be substituted. This is in spite of the fact that experimental evidence has meanwhile given some support not only for the usefulness but also for the reasonableness of the suggested relation.

Attention is here called to some of the present results for the mixing component as compared to those obtained by other methods.

A numerical solution has been developed for the shear region between two parallel streams at different free stream velocities. The validity of the method developed has not been experimentally verified but the results seem reasonable. Comparison with the asymptotic solution (2) as shown in figure 5 indicates good agreement with the present analysis based on the representative "j" streamline velocity. Both curves are for zero initial boundary layers. This, of course, does not give credulence to the solution in the developing region but indicates that the final profile is reasonable.

Shown in figures 6 and 7 are plots of velocity profiles from the initial point of mixing through a length equivalent to the presently investigated cavity. The picture shown by the plots is what would be expected from a physical reasoning, that is a smoothing out of the profile and a spreading of the shear region.

It would seem that the only question is if the development takes place too rapidly or too slowly. Any adjustment that might be required in the development length would not depend on the basic solution but on the representation of the empirical eddy viscosity ratio and the initial value of eddy viscosity. These terms have been under investigation for a long period by several researchers (e.g., NASA grant No. NsG 13-59 at the University of Illinois) and perhaps further investigation of the problem using the present solution will provide a more indicative relation for the eddy viscosity. An investigation is being conducted as a part of the present research effort to extend and more fully verify the results of the two-stream solution and to establish an eddy viscosity relation on a firm experimental basis. Although there is some degree of uncertainty, the resultant mixing model has proved useful in the study of cavity flow and heat transfer. The analysis could also be used to calculate wakes of airfoils or any sharp trailing edge body. In addition, the analysis provides a standard numerical solution against which less rigorous but more easily used engineering solutions may be compared.

Using the energy balance systems analysis with the present restricted method of calculating the wall heat transfer provides a reasonable agreement for cavity bulk temperature in a cavity with constant wall temperature or step changes. Figure 13 shows a comparison of data for three mass bleed rates with constant cavity wall temperature. Also, presented in figure 14 are data for a cavity wall with two step changes in temperature after the initial change at the leading edge. The data are in generally good agreement with the analysis and follow the trend of the curves well. This indicates that the analytical model gives a reasonably useful tool in the study of flow over and within nearly circular cavities.

Reynolds (13) suggested that the local heat transfer coefficient for a flat plate with constant heat flux is 4.3 per cent greater than for a flat plate with constant wall temperature. Using this factor the analytical results for the constant temperature wall were shifted and data for the constant flux case was then compared with this shifted result in figure 15. Agreement is fair and the curves are only an indication as the shifting factor was derived for constant initial conditions to the plate. A method of calculating local temperature for constant wall flux similar to the method for constant wall temperature would, of course be more reliable.

Local heat transfer coefficients for the cavity wall are presented in figures 16, 17, and 18 for the isothermal case. The first plot is normalized with an average heat transfer coefficient (see nomenclature for definition). For this plot, the temperature difference for the local and average coefficient was considered to be the constant wall temperature minus the cavity bulk temperature, T_{ob}. All data lie together and indicate the same heat transfer pattern from the wall as the total amount of heat transferred was changed. Only three sets of data were plotted but the other results fall in the same distribution. Note the uncharacteristic rise in heat transter at the separation point due to the mixing zone.

It is interesting to note that the average heat transfer coefficient is nearly proportional to the Length Reynolds number to the -2/5 power. This is in agreement with Larson (14) and his axisymmetric model and in disagreement with Fox (17) and his rectangular model. This is not conclusive as data were taken for only one value of Reynolds Number.

In figure 17, the normalizing factor is the heat transfer coefficient of a flat plate equivalent to the cavity wall. This plot then indicates quantitatively the deviation of the cavity wall heat transfer from that of a flat plate. The data shifts, retaining the heat transfer pattern, depending on total heat transferred to the cavity or the cavity temperature. If the heat transfer were completely like a flat plate, all data would be on an ordinate value of one. Note that there is generally a deficiency in total amount of heat transferred and that for the higher value of T_{ob}, there is a greater deficiency. This is due to the non-uniform temperature profile at the start of the wall. Note also that the bleed flow rate does not directly influence the results except through the bulk temperature. The coefficient decreases at the trailing edge, or separation edge, which is not characteristic of a flat plate. This is due to the effect of the mixing region across the cavity opening which might be considered a trailing end effect. The sharp increase at the reattachment point is, of course, due to the reattachment of the jet on the cavity wall.

A total heat transfer coefficient for an equivalent flat plate (that is a plate of the same length as the cavity opening, ℓ_m) was used as the normalizing factor in figure 18. This plot then provides a means of comparison of the heat transfer in a cavity with mass bleed to the equivalent total heat transfer from a flat plate of comparable length.

In figures 19, 20, and 21 local heat transfer coefficient data are shown for two interior wall temperature step changes. These show the same general trends and agreement as for the isothermal wall but also indicate the sharp temperature changes at the steps and the influence on the over-all heat transfer pattern when compared to the isothermal data.

Shown in figure 22 are data for a simulation, by a line source at the confluence point, of the wall heat transfer. The data were taken for this study on a model used by Miles (4) and modified for introducing mass bleed into the cavity. The curves indicate that the data are considerably lower than results predicted by the present analysis for a constant wall temperature heat transfer with the same total heat transferred. The second set of curves is for Miles' analysis modified to account for mass bleed. This analysis was derived as if the heat transferred from the wall acts as a line source at the point of confluence and the data fit the analysis rather well.

The finite size and location of the heating element as compared to the sharp edge of the cavity probably caused more heat to be transferred from the cavity than for the case of actual wall heat transfer. Korst has pointed toward this possibility (1). In addition, the plot would seem to indicate a deficiency in the former analysis, especially in the wall heat transfer simulation technique.

V. CONCLUSIONS AND RECOMMENDATIONS

It has been shown that the numerical calculations based on the proposed model produce reasonable results for either the constant wall temperature case or for step changes in wall temperature. It is expected that the method of analysis could be extended to higher wall and bleed temperatures and larger bleed rates which would result in higher bulk temperatures. The analysis is also applicable to temperatures lower than the free stream.

To be able to extend the results to a more general case of complete non-uniform wall temperatures, a better method of predicting the temperature profile along the wall must be determined. This is necessary in predicting the local wall heat transfer along a non-isothermal wall and in determining the initial temperature profile to the two-stream mixing calculation. A study should be conducted investigating both experimentally and analytically the temperature distribution along a non-isothermal flat plate. The results of this study could then be readily incorporated in the present analysis and additional data could be obtained with the present experimental cavity and related equipment.

A further investigation should be made of the empirical eddy viscosity relation for two-stream mixing. This could be done by making velocity and temperature profile measurements in a well defined mixing region (without the complicating influence of a cavity) and the results then used in the cavity analysis by simply changing the present relationship for eddy viscosity. The cavity wall causes the secondary stream to merge at an angle with respect to the primary stream and introduces a further complicating variable that could be investigated after the more simple case has been examined. This type of an investigation would also contribute to a better understanding of eddy viscosity and turbulent flow in general.

The experimental apparatus as designed and used in this investigation will allow further data to be taken for the most general case of a completely arbitrary wall temperature. Using this equipment an investigation might be conducted to determine the effect of a heat source along the cavity wall on the bulk temperature. This could be done by using one or more heaters and varying the location along the wall.

A further investigation might be performed by heating non-isothermally a variable length leading plate to the cavity. This would indicate the effect of the temperature and velocity initial conditions of the primary stream on the flow over and within a cavity.

NOMENCLATURE

SYMBOLS

A	-	a/ℓ_m
a	-	location of ramp
B	-	b/T_{ob}
b	-	step change in wall temperature
C^2	-	Crocco Number, $u^2/2C_p\,T_o$
C_p	-	specific heat
$E_{D_{bl}}$	-	energy dissipated in wall boundary layer
E_{D_m}	-	energy dissipated in mixing region
E_{D_L}	-	energy dissipated in core region
E_{D_R}	-	energy dissipated in recompression zone
E_t	-	net transfer of mechanical energy to cavity fluid
e_D	-	local rate of dissipation per unit volume
G	-	bleed rate
k	-	thermo conductivity
J	-	total number of step changes in cavity wall temperature
L	-	ℓ/ℓ_m
	-	location of steps or cavity lengths
M	-	$m\ell_m/T_{ob}$
m	-	slope of ramp temperature changes in cavity wall temperature
N	-	total number of ramps
n	-	boundary layer power law coefficient

Q_d	-	heat diffused to free stream
Q_m	-	heat transferred across mixing region
Q_w	-	heat transferred to boundary layer along cavity wall
$\overline{Q}_w$	-	normalized Q_w, $Q_w/\ell_m \rho_a u_a C_p T_{oa}$
Q_w	-	average heat transfer from cavity wall, $Q_w = Q_w(\ell_w/\ell_m)$
$q(x)$	-	local heat transfer along wall
r	-	upper limit of incomplete beta function, $1 - (a/x)^{9/10}$
T	-	temperature
$\overline{T}$	-	average temperature
u	-	velocity in x direction
v	-	velocity in y direction
V	-	volume
W_m	-	shear energy transferred across mixing jet
x,y	-	intrinsic coordinates or cavity wall coordinates
δ	-	boundary layer thickness
ϵ_t	-	eddy diffusivity
η	-	coordinate of similarity mixing profile
Λ	-	stagnation temperature ratio in mixing profile
ν	-	kinematic viscosity
ξ	-	x/δ_o
ψ	-	stream function
ρ	-	density
τ	-	shear stress
σ	-	similarity parameter for similarity mixing region

ϕ	-	dimensionless velocity
θ	-	boundary layer momentum thickness
ω	-	y/δ_o

SUBSCRIPTS

a	-	free stream conditions
b	-	bulk cavity conditions
d	-	discriminating streamline
j	-	jet boundary streamline
m	-	mixing
o	-	total conditions (e.g., total temperature) or origin of mixing region
s	-	bleed
T	-	isothermal flat plate
w	-	wall
δ	-	boundary layer thickness

PARAMETERS

B_{r_n}	-	incomplete Beta function, figure 9
$\overline{G}_s$	-	normalized bleed rate into cavity
h	-	$Q_w/A_{total}(T_w - T_{ob})$
h_{fp}	-	$0.0296\ c_p \rho_b u_b (Re_m \phi_b \frac{x}{\ell_m})^{-1/5}$
h_{efp}	-	$0.037\ c_p \rho_a u_a Re_m^{-1/5}$
$h(\xi;x)$	-	local heat transfer coefficient with step temperature changes
$I_1(\eta)$	-	see p. 49
$I_3(\eta)$	-	see p. 49

$I_4(\eta)$ - see p. 25

Pr_t - Turbulent Prandtl Number

Re_m - Mixing Length Reynolds Number

Re_x - Local Reynolds Number along cavity wall

Re_δ - $u_a \delta_o / \nu$

St_w - Average Wall Stanton Number,

M - $(\Delta\bar{\psi})^2 Re_\delta / \Delta\xi\bar{\epsilon}$

E - Pr_t M

$\bar{\epsilon}$ - ϵ_t / ν

$\bar{\bar{\epsilon}}$ - $\epsilon_t / \epsilon_{t_o}$

$\bar{\psi}$ - $\psi / \rho_a u_a \delta_o$

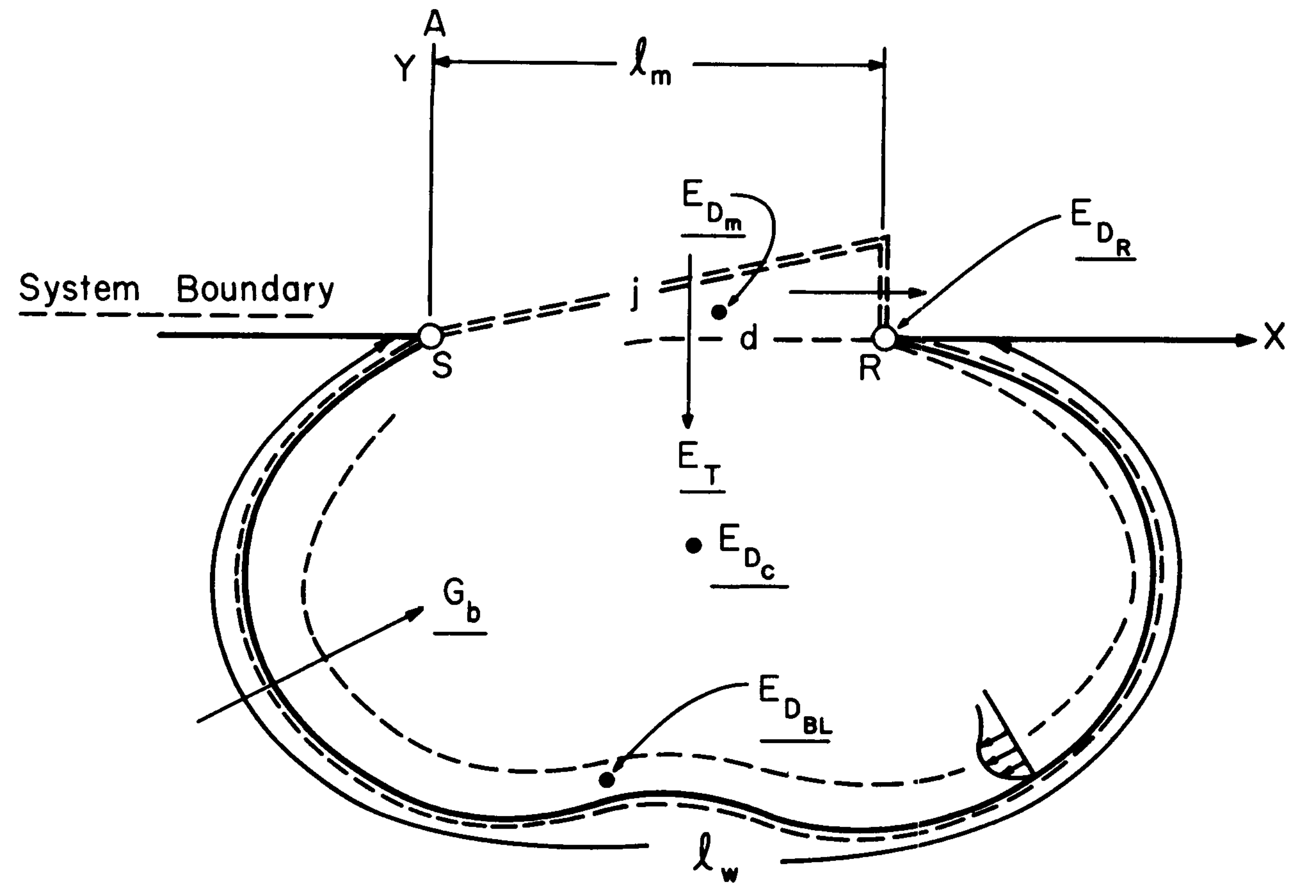

$$\int_0^{\ell_m} \tau_j U_j \, dx - \frac{1}{2}\int_{y_j}^{y_j} \rho U^3 \, dy = \int_V e_D \, dv = E_{D_m} + E_{D_R} + E_{D_{BL}} + E_{D_c}$$

Figure 1. Cavity Dissipative Model

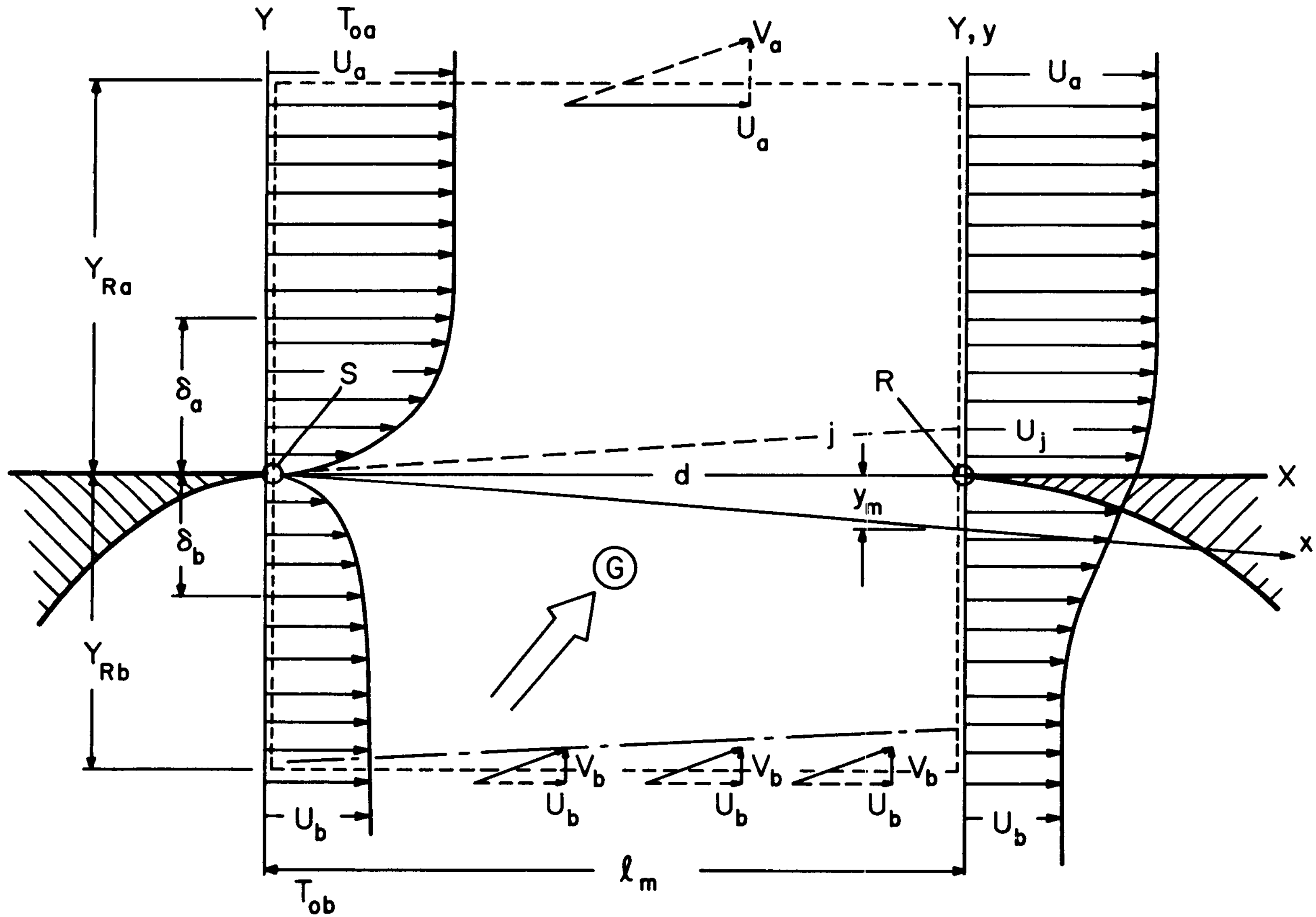

Figure 2. Two-stream Mixing Components of the Cavity Model

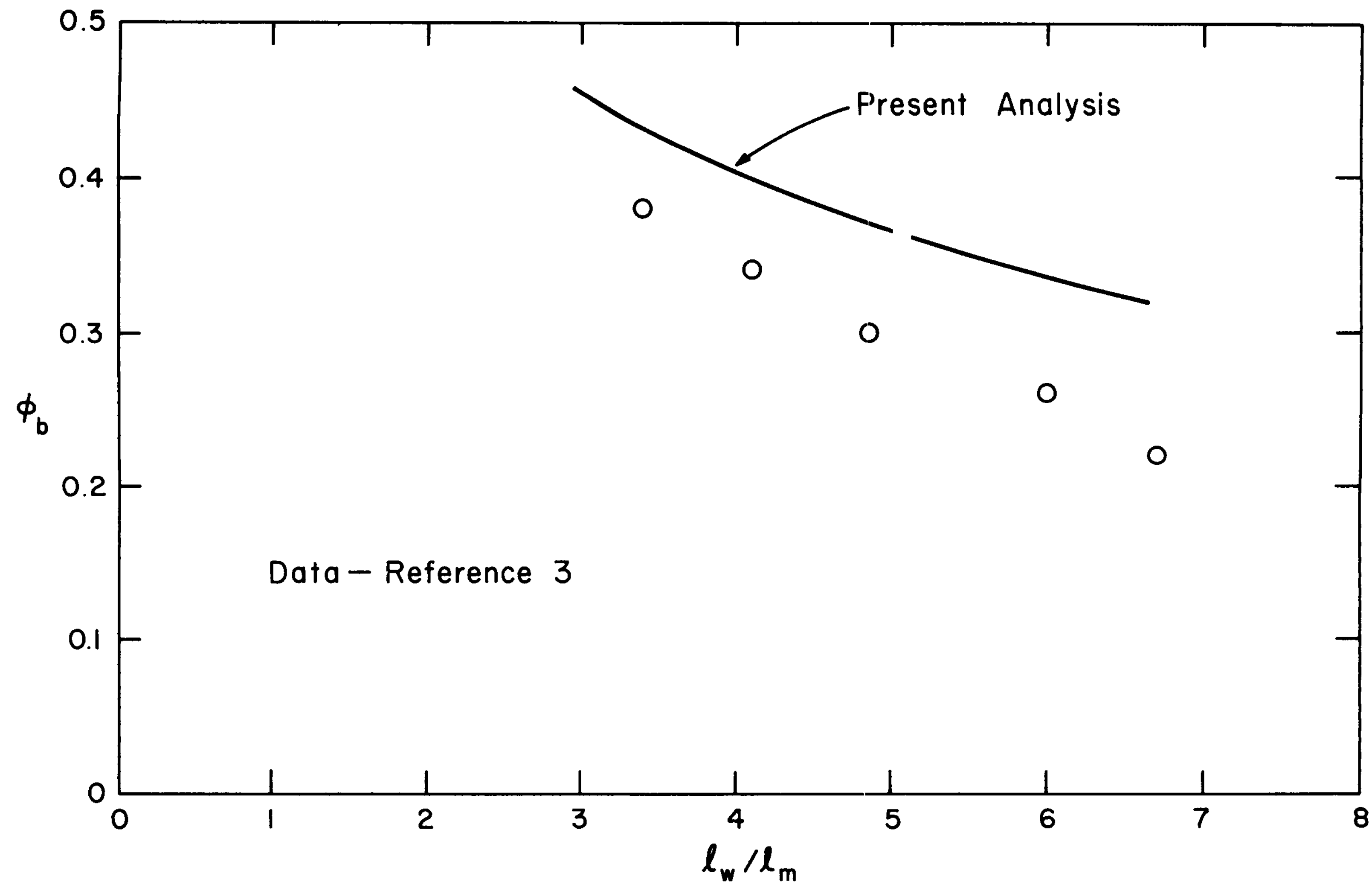

Figure 3. Comparison of Analytical Cavity Reference Velocity to Golik's (3) Experimental Data

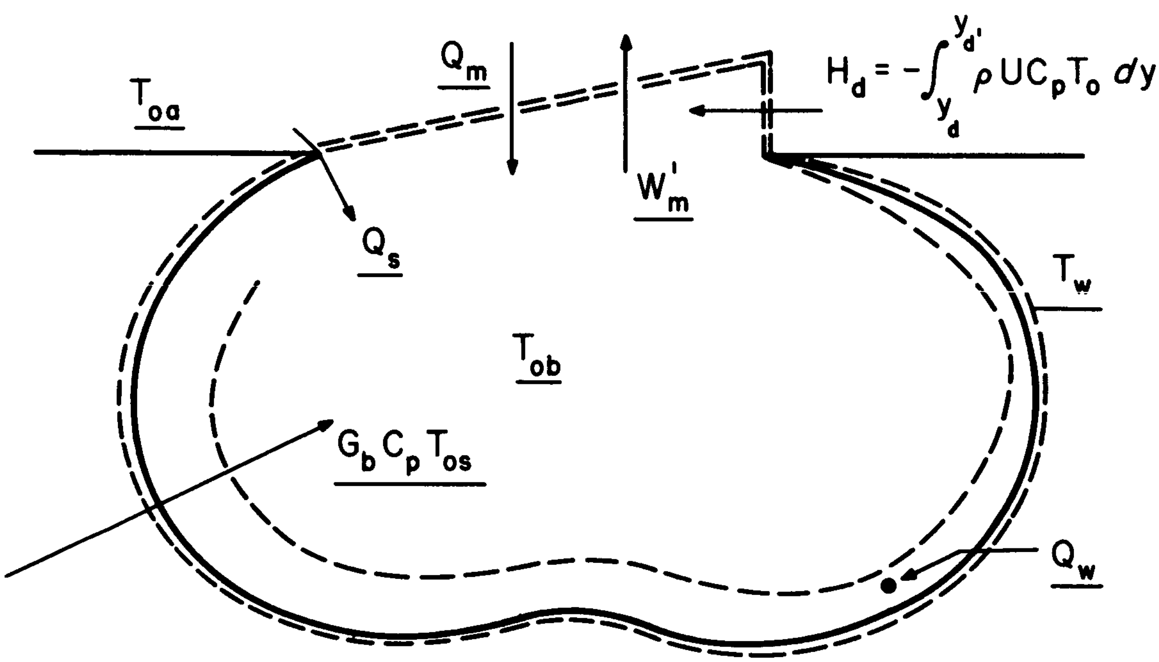

$$Q_w + G_b C_p T_{os} + Q_s + (Q_m - W'_m) + H_d = 0$$

Figure 4. Cavity Heat Transfer Model

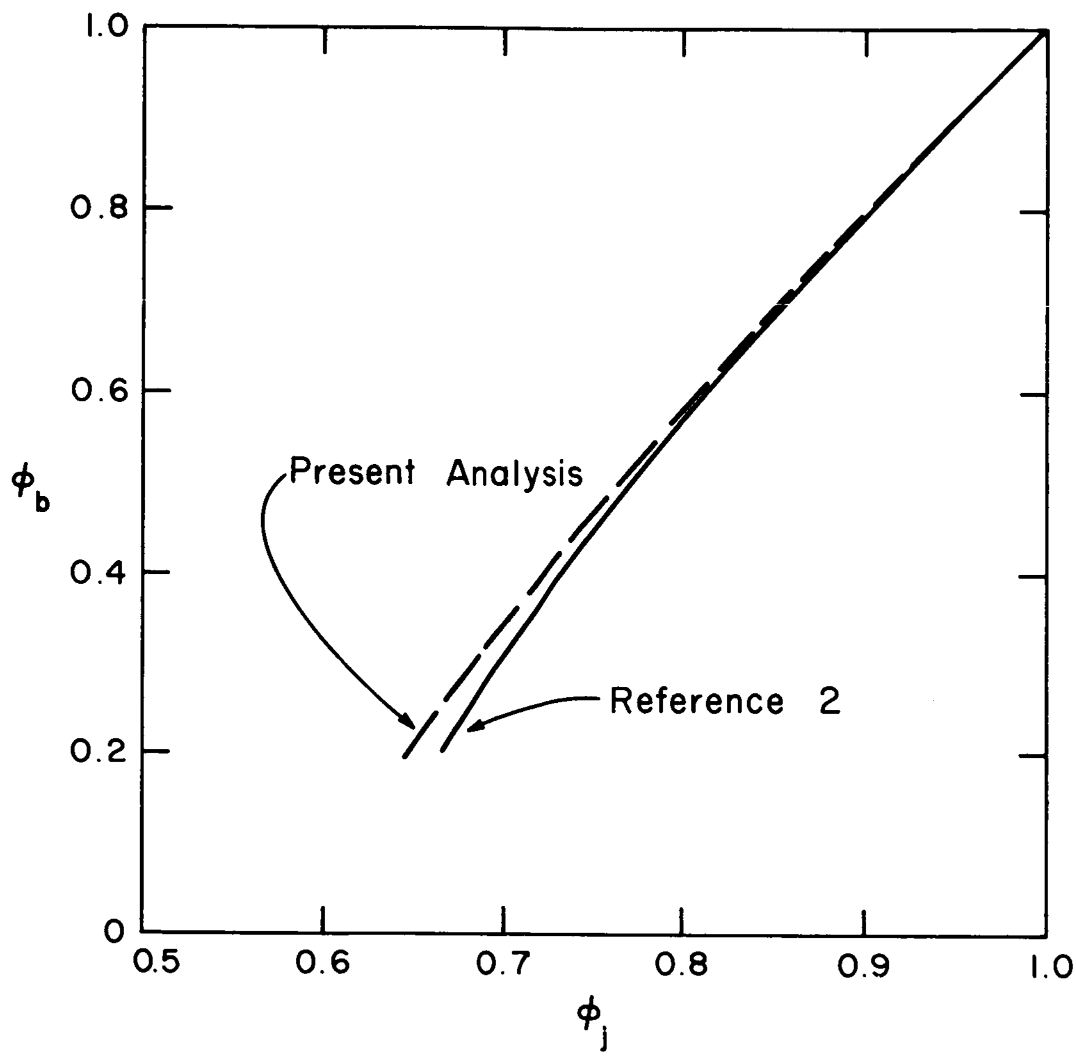

Figure 5. Comparison of Present Two-stream Analysis with Results of Ref. 2

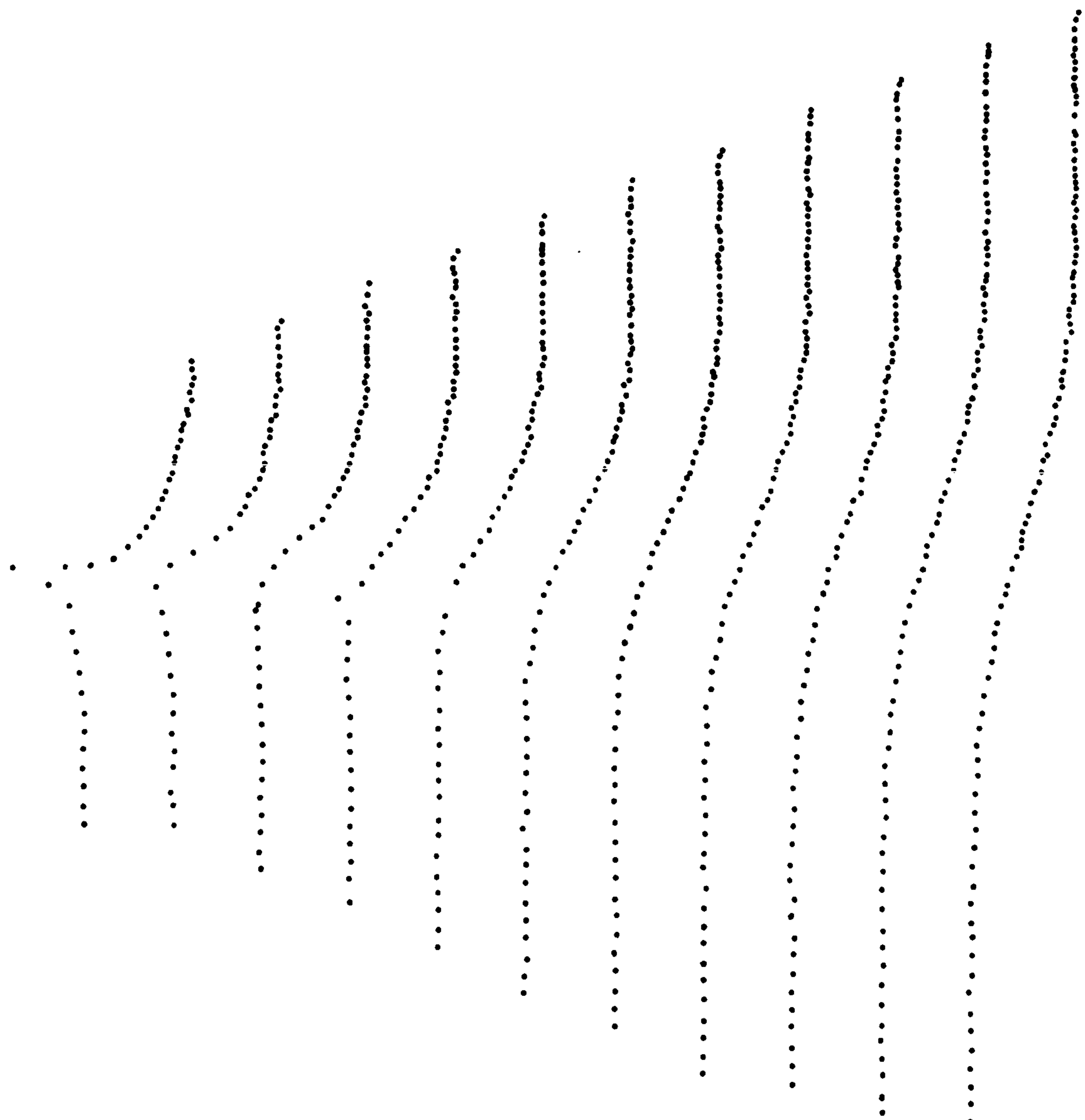

Figure 6. Developing Velocity Profile to Point of Reattachment (Initial Boundary Layers)

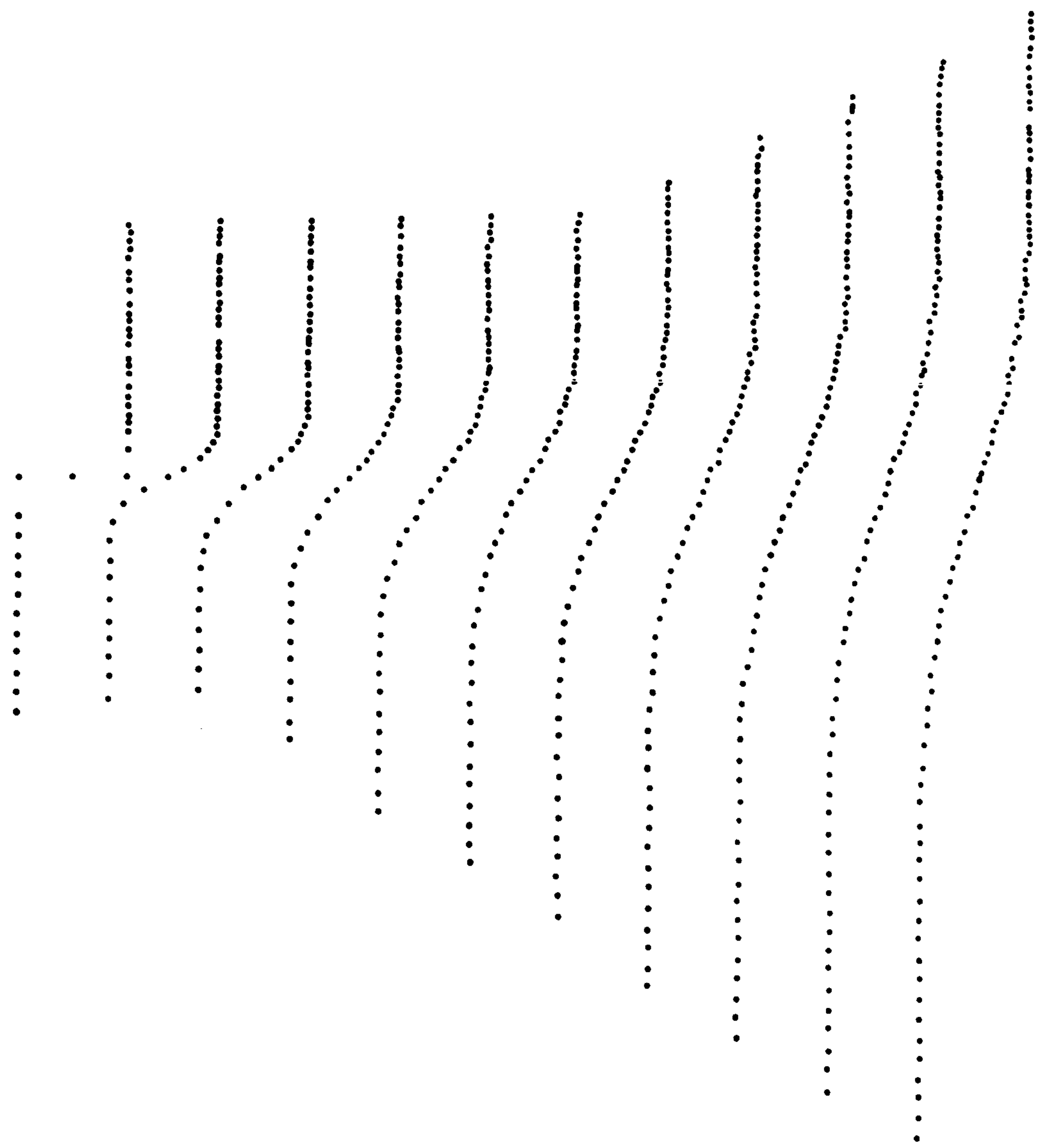

Figure 7. Developing Velocity Profile to Point of Reattachment (No Initial Boundary Layers)

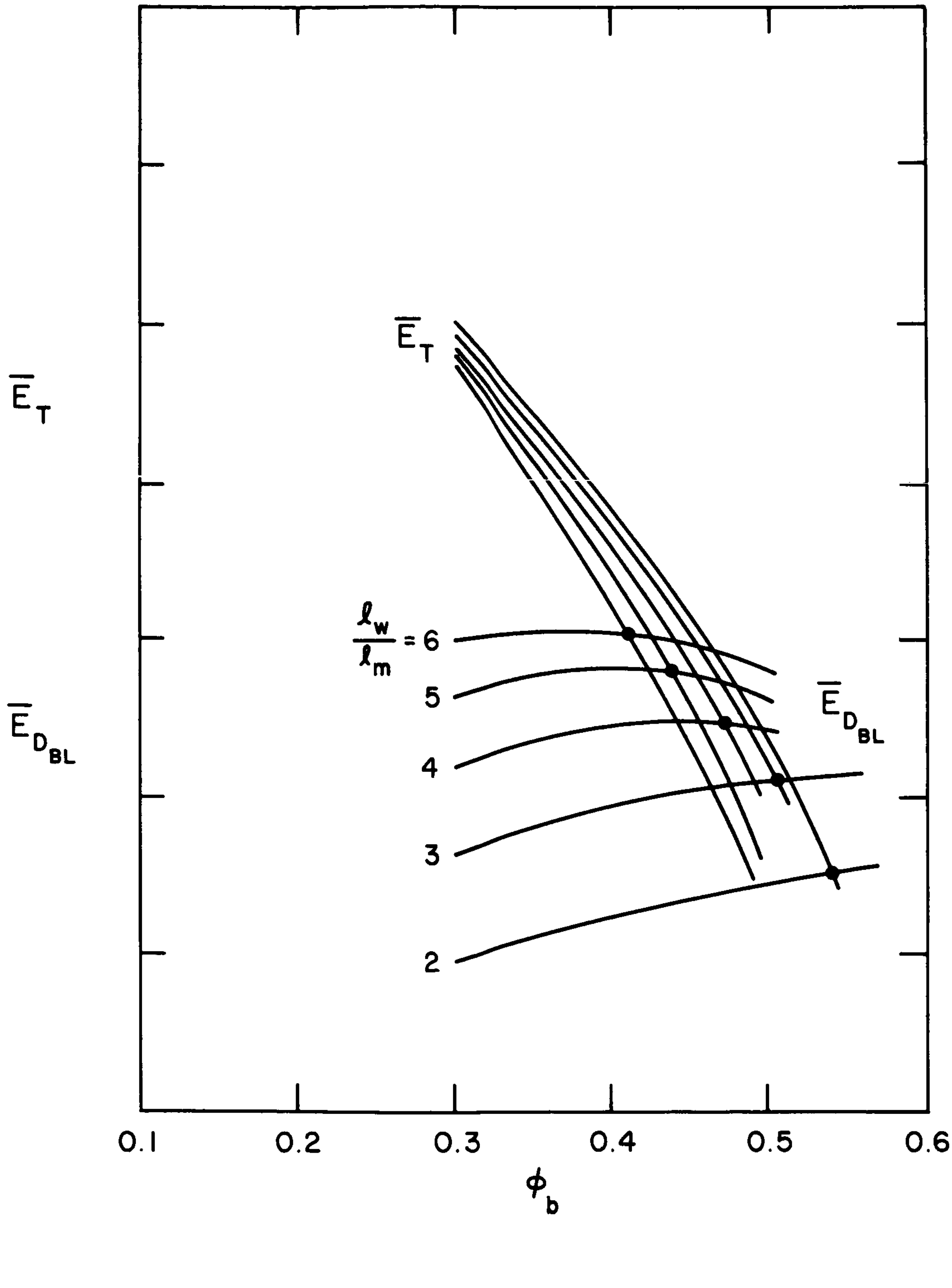

Figure 8. Mechanical Energy Balance for Cavity

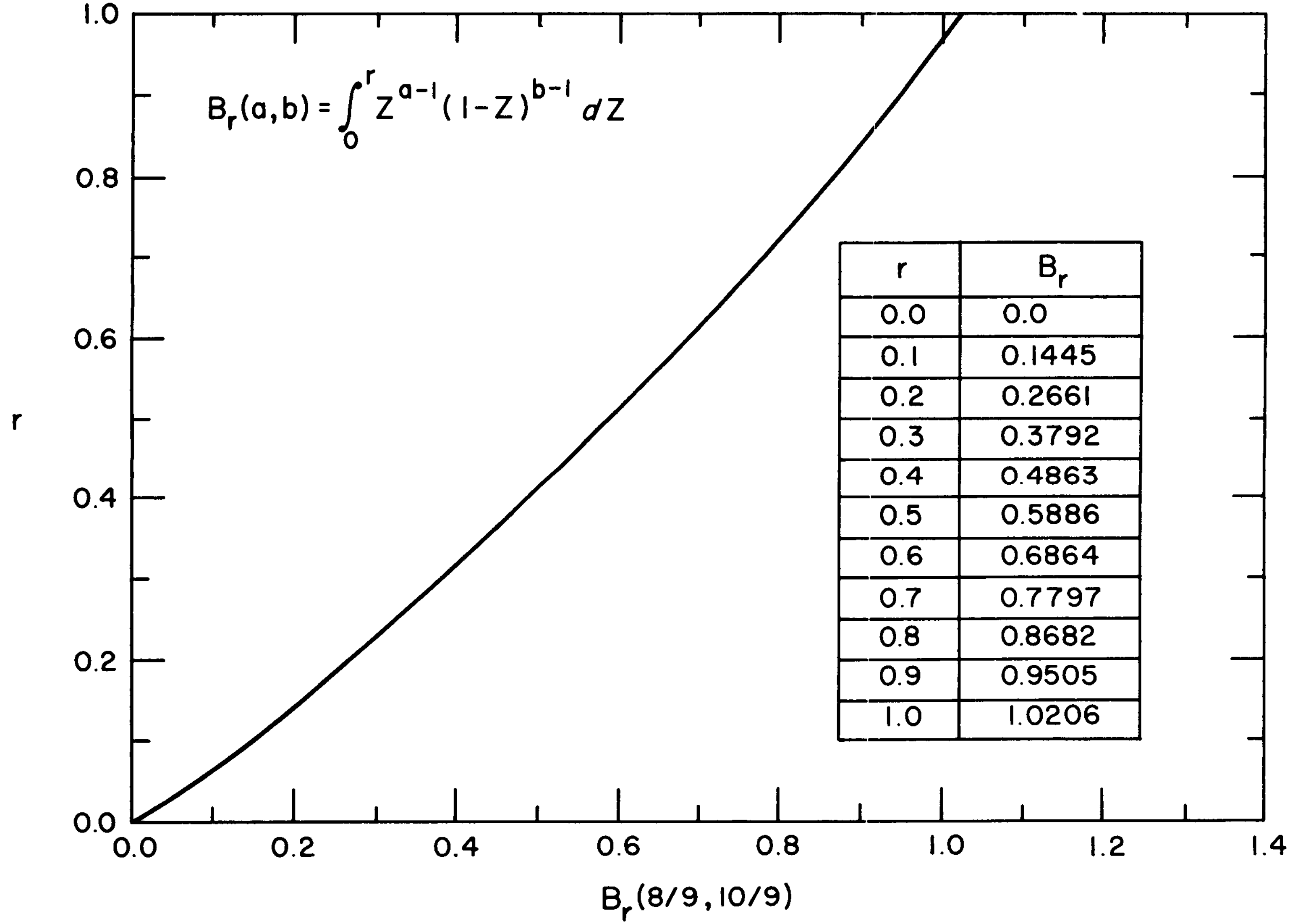

r	B_r
0.0	0.0
0.1	0.1445
0.2	0.2661
0.3	0.3792
0.4	0.4863
0.5	0.5886
0.6	0.6864
0.7	0.7797
0.8	0.8682
0.9	0.9505
1.0	1.0206

Figure 9. Incomplete Beta Function, $B_r(8/9, 10/9)$

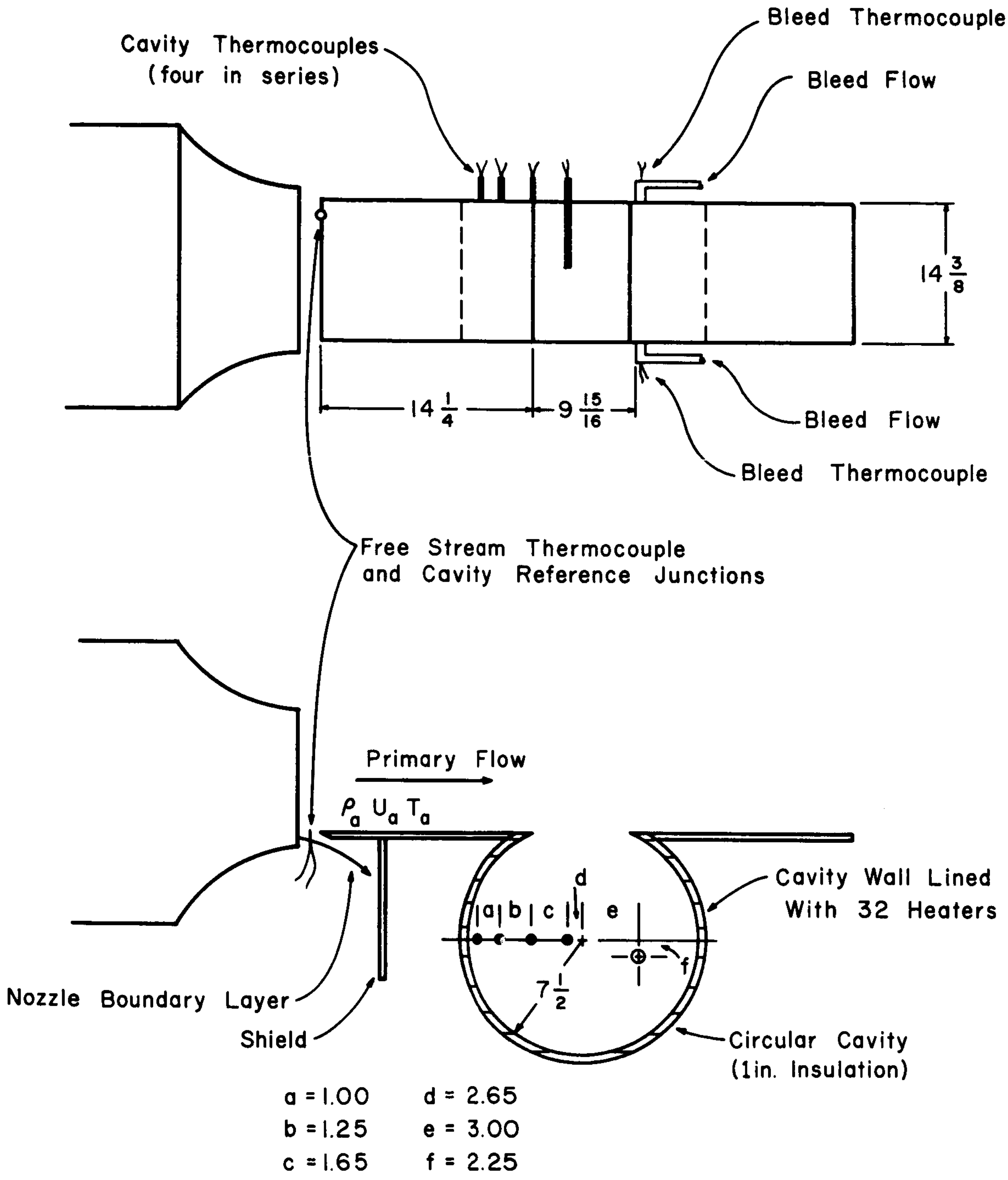

Figure 10. Schematic of Experimental Facility Showing Thermocouple Locations Inside and Outside of Cavity

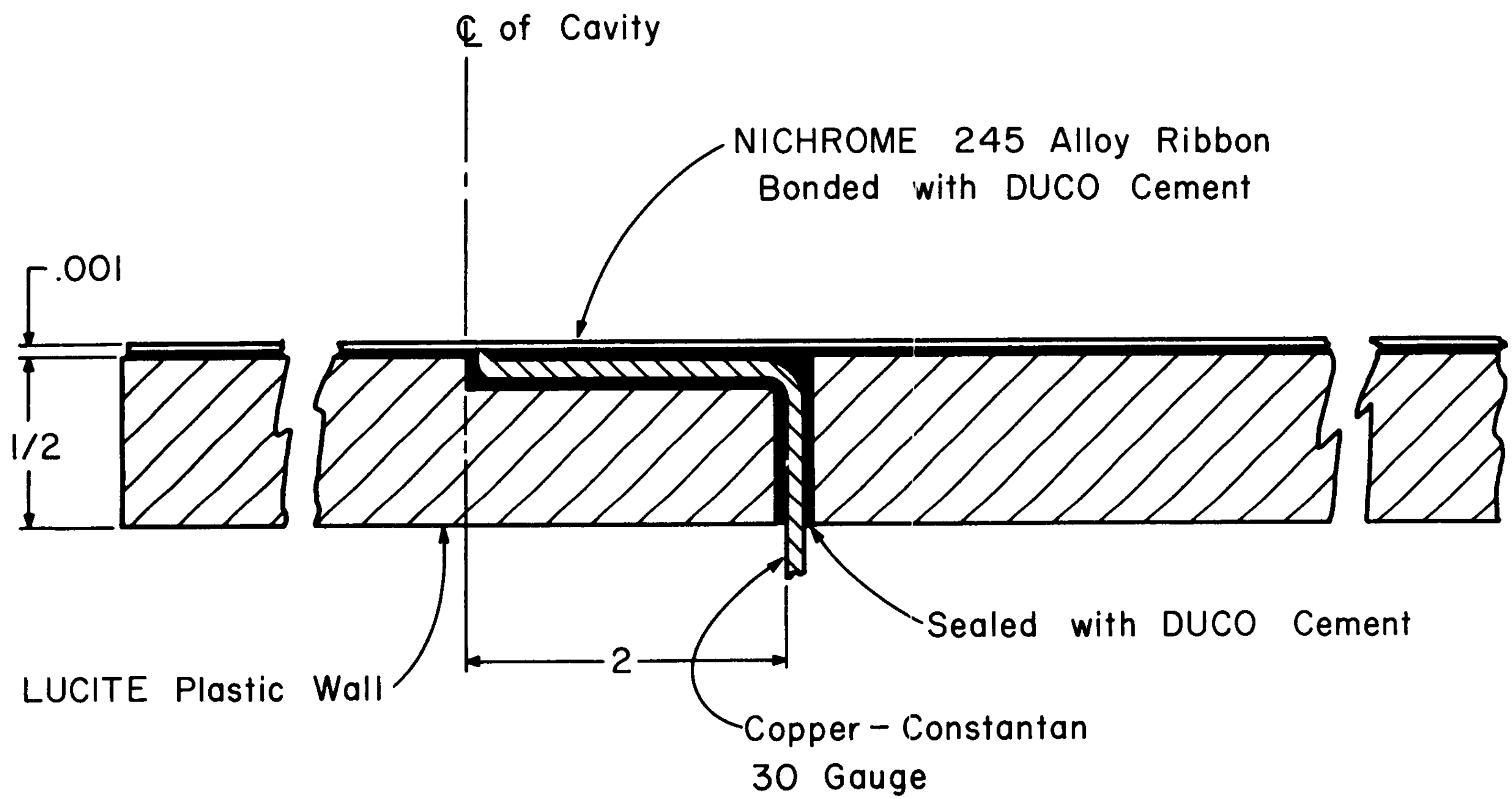

Figure 11. Sketch of Thermocouple Mounting in Cavity Wall

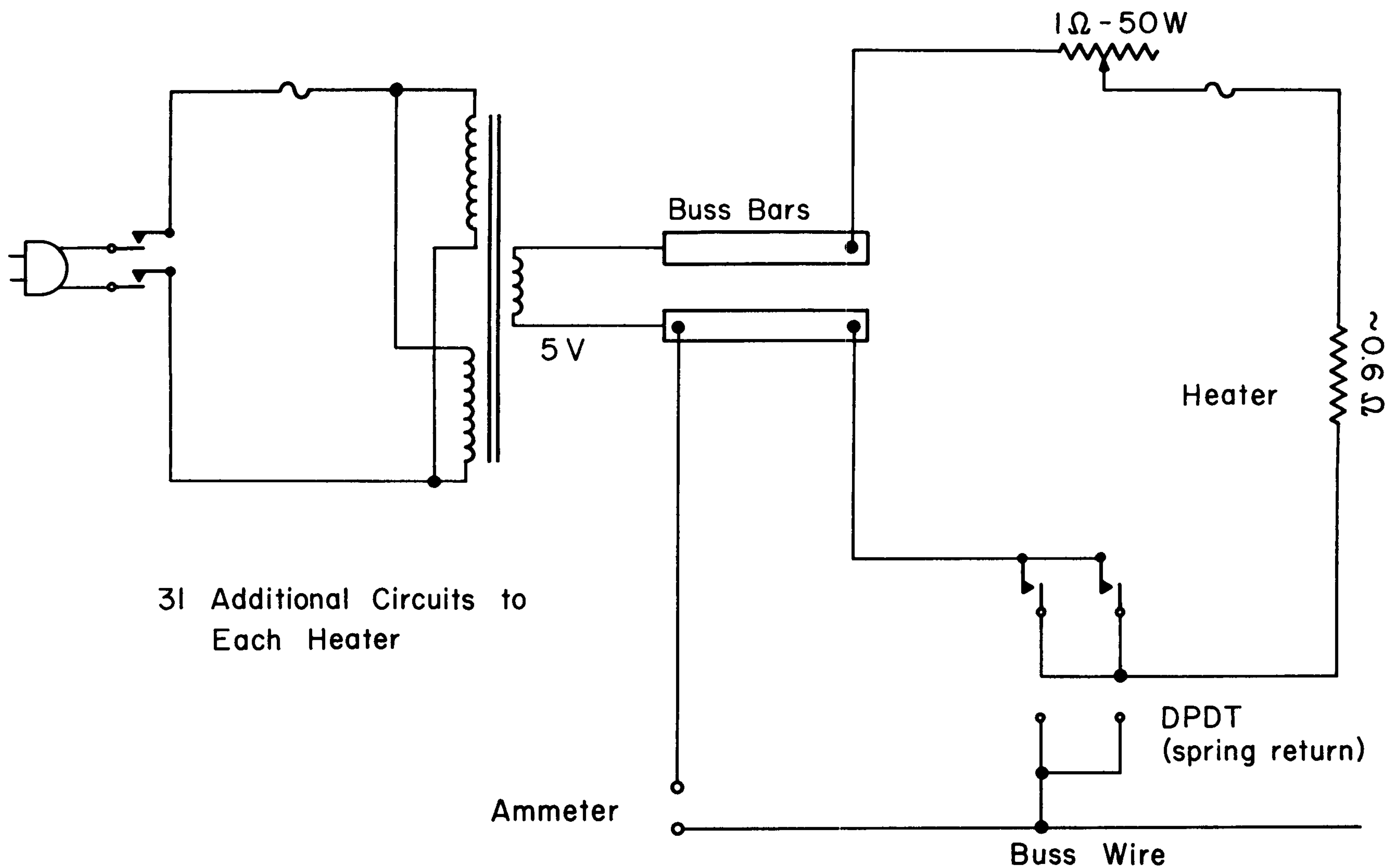

Figure 12. Schematic of Heater Control

PAGE 83 IS MISSING FROM THE ORIGINAL DOCUMENT.

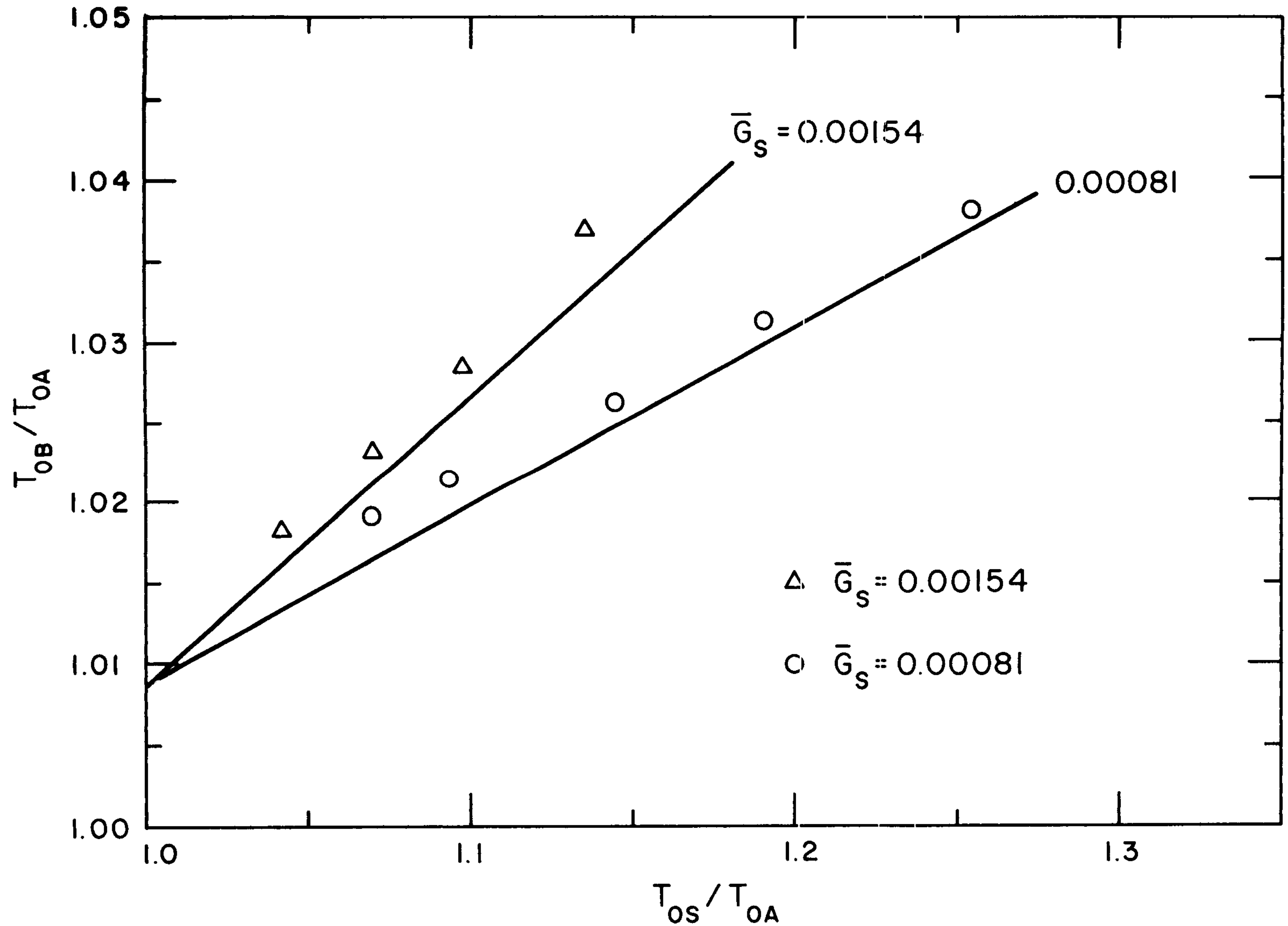

Figure 14. Bulk Temperature vs Bleed Temperature for Different Bleed Rates (Two-step Changes in Wall Temperature)

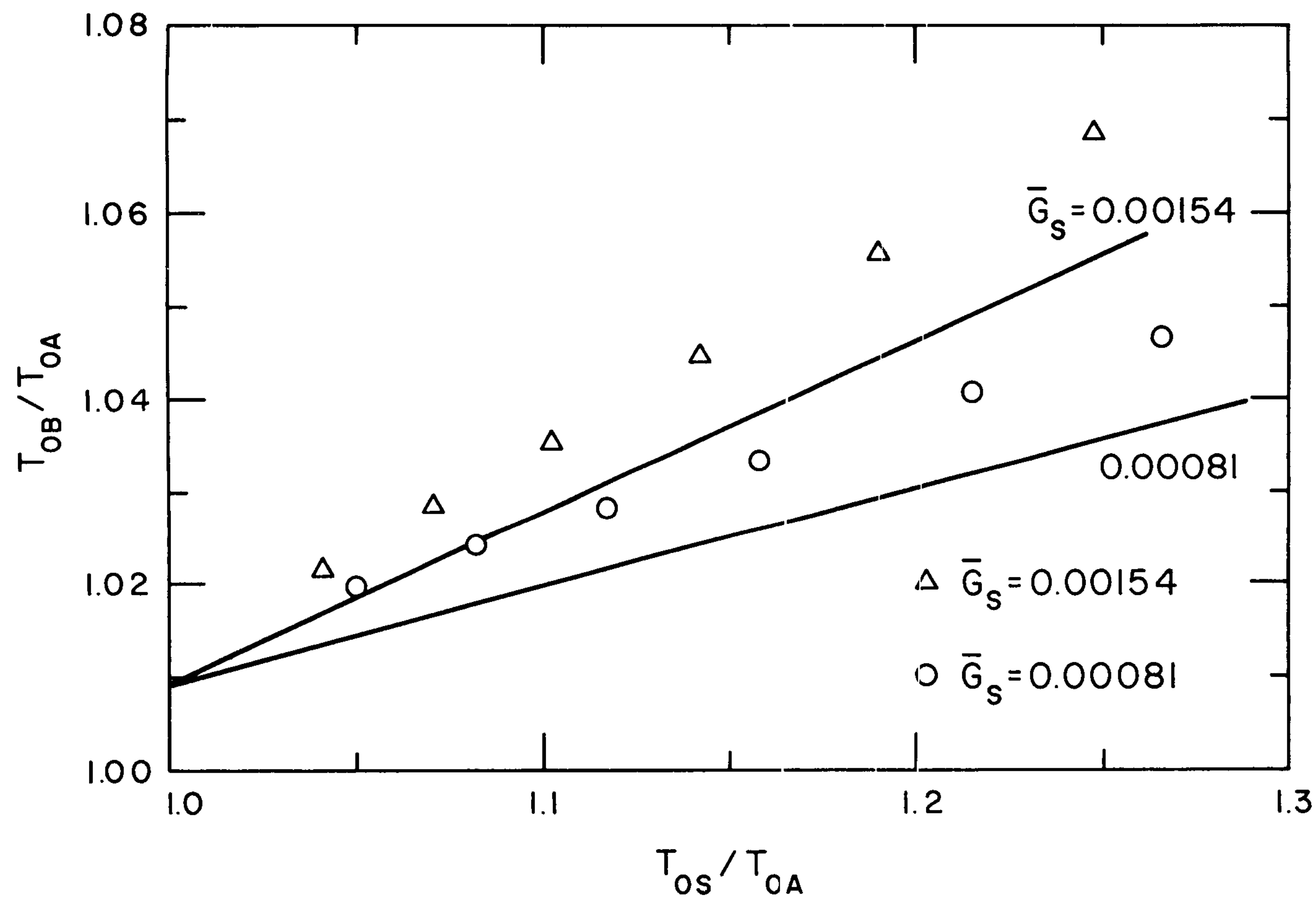

Figure 15. Bulk Temperature vs Bleed Temperature for Different Bleed Rates (Constant Flux along Wall)

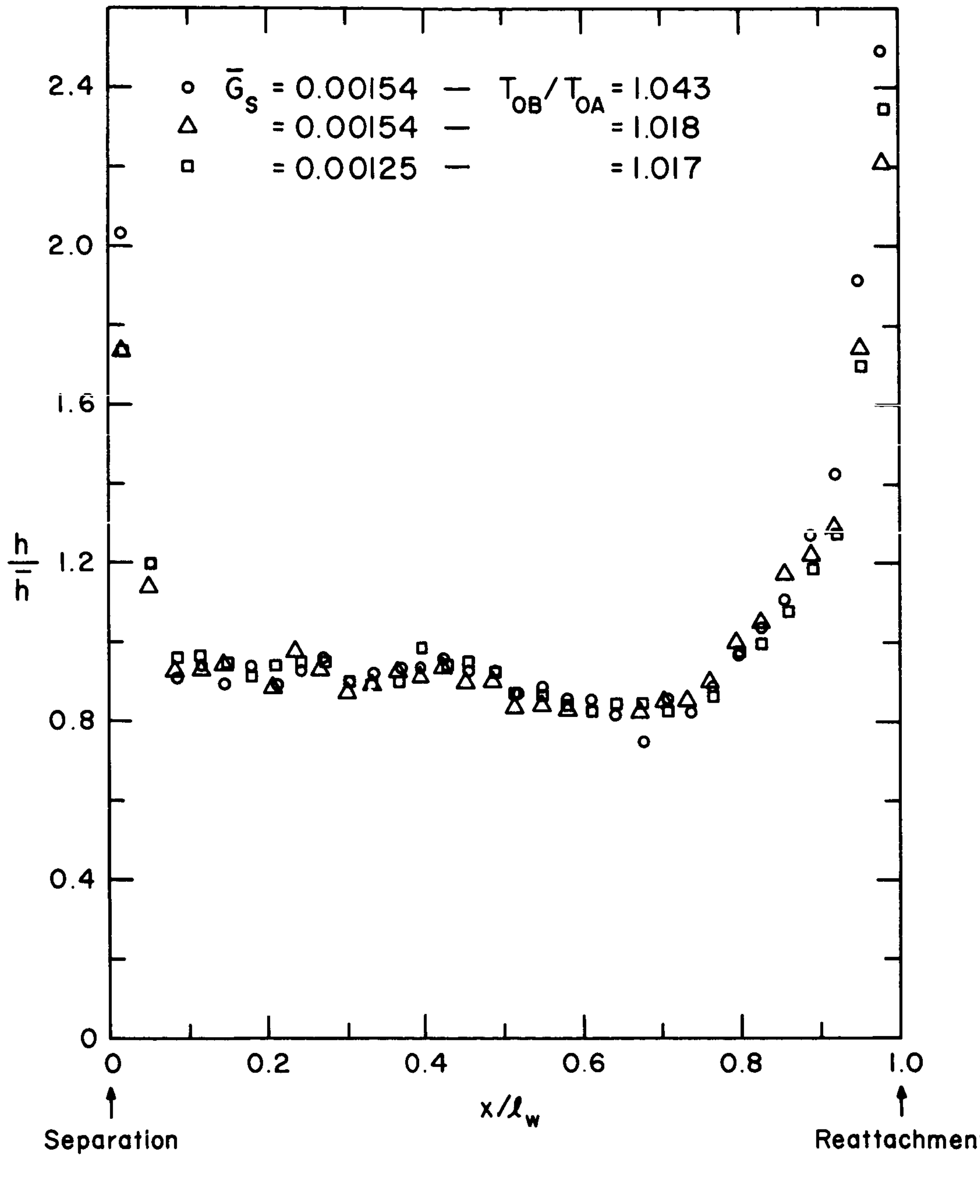

Figure 16. Local Heat Transfer Coefficient/Average Coefficient (Isothermal Wall)

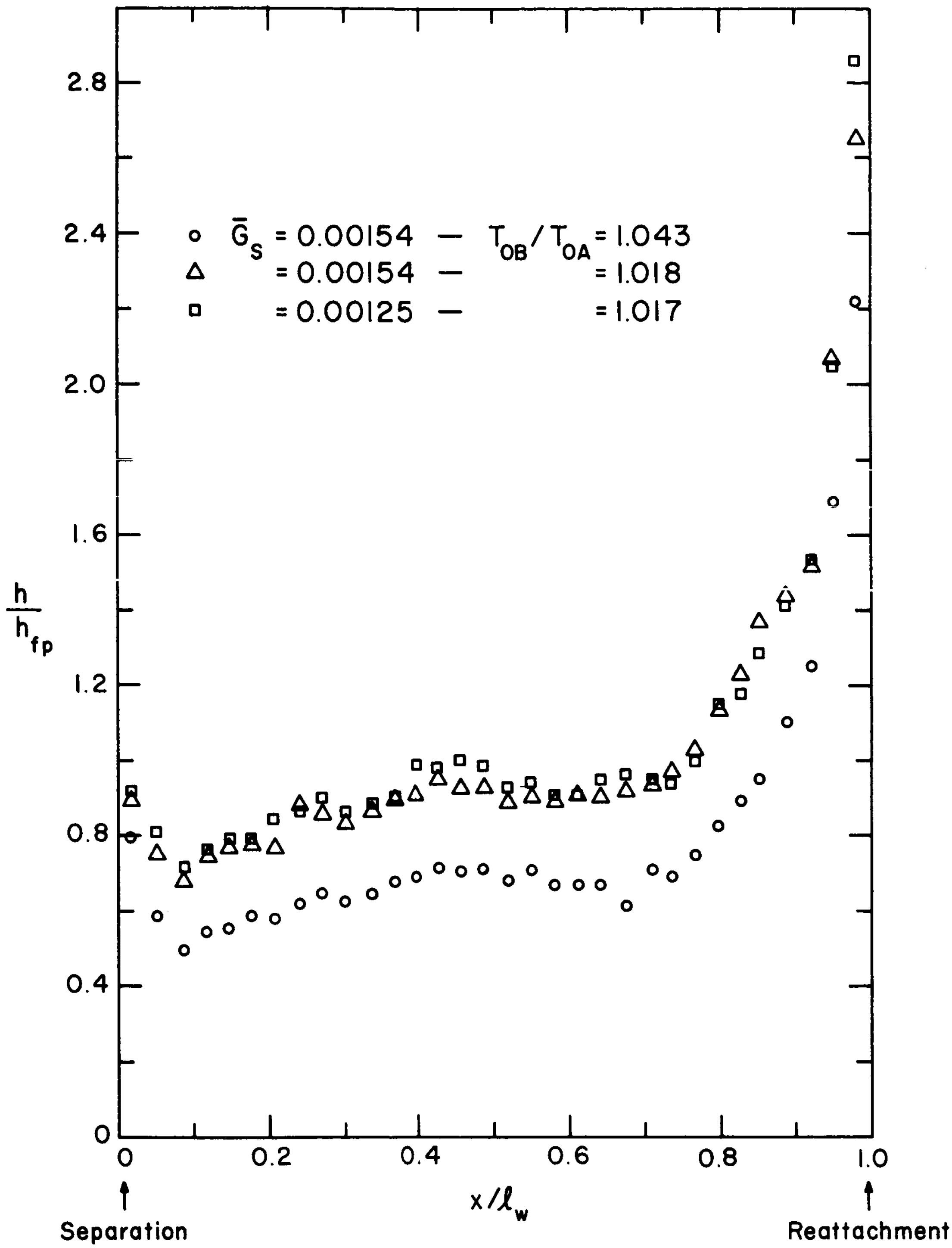

Figure 17. Local Heat Transfer Coefficient/Local Flat Plate Coefficient (Isothermal Wall)

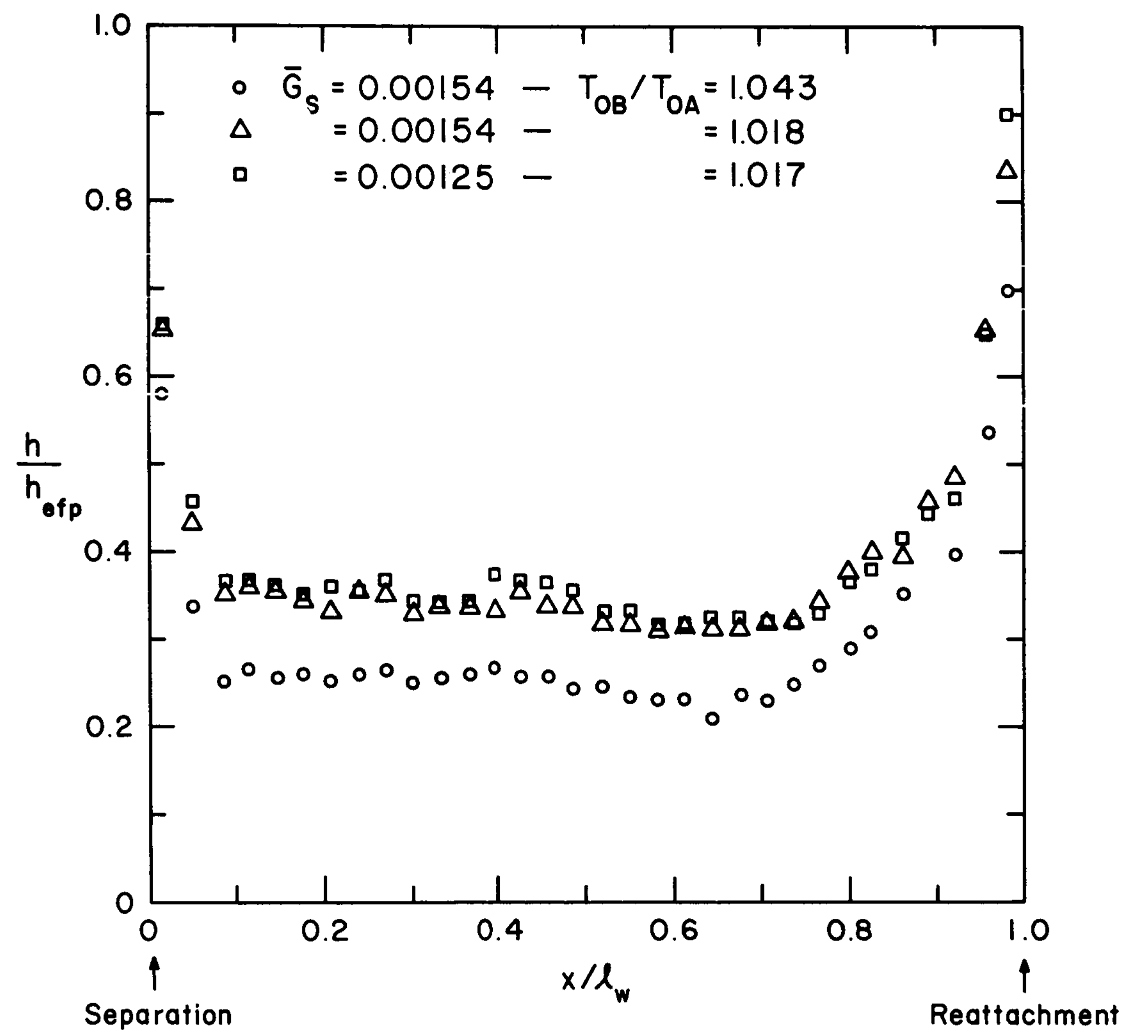

Figure 18. Local Heat Transfer Coefficient/Equivalent Mixing Length Flat Plate Coefficient (Isothermal Wall)

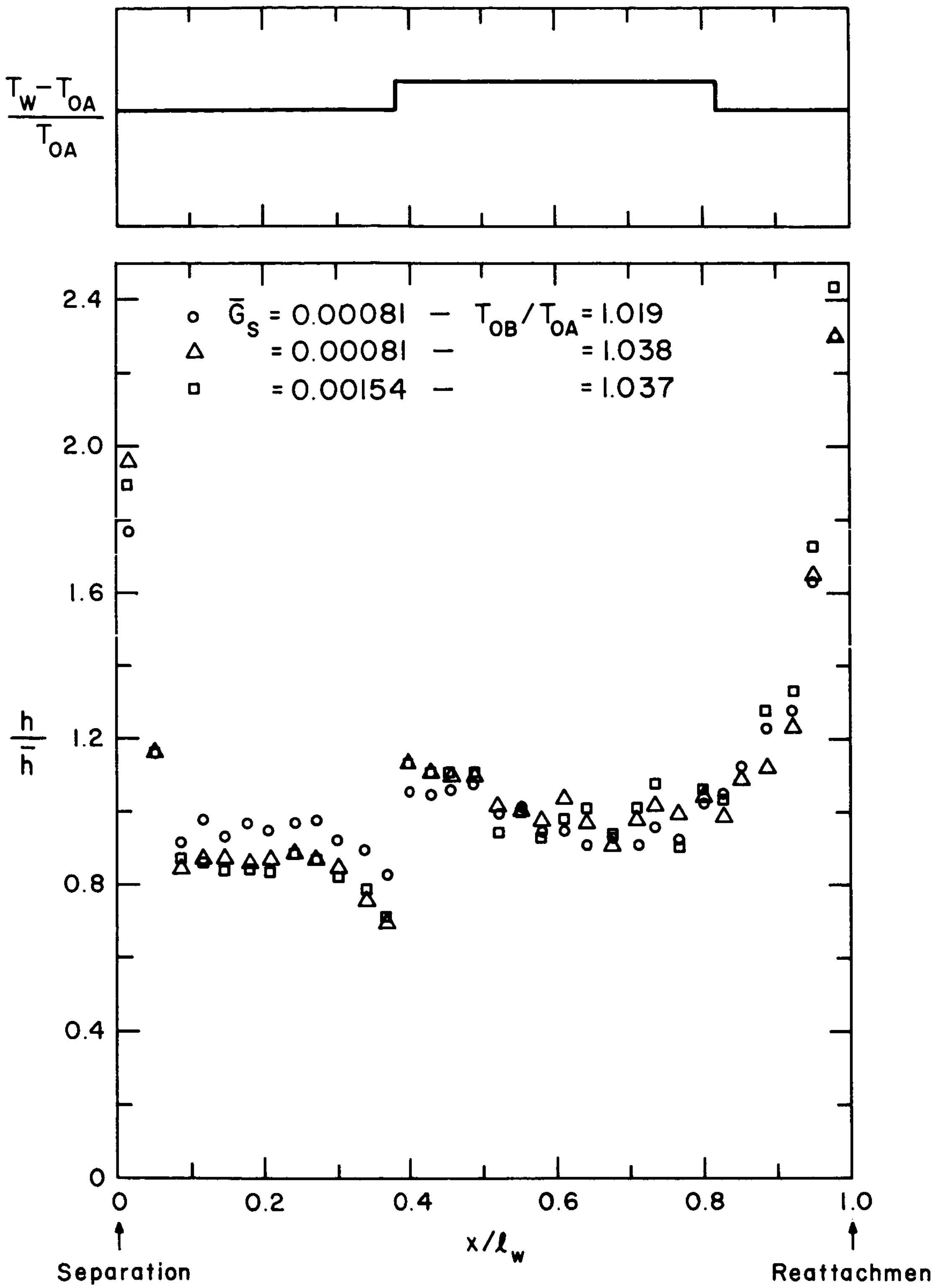

Figure 19. Local Heat Transfer Coefficient/Average Coefficient (Two-step Changes in Wall Temperature)

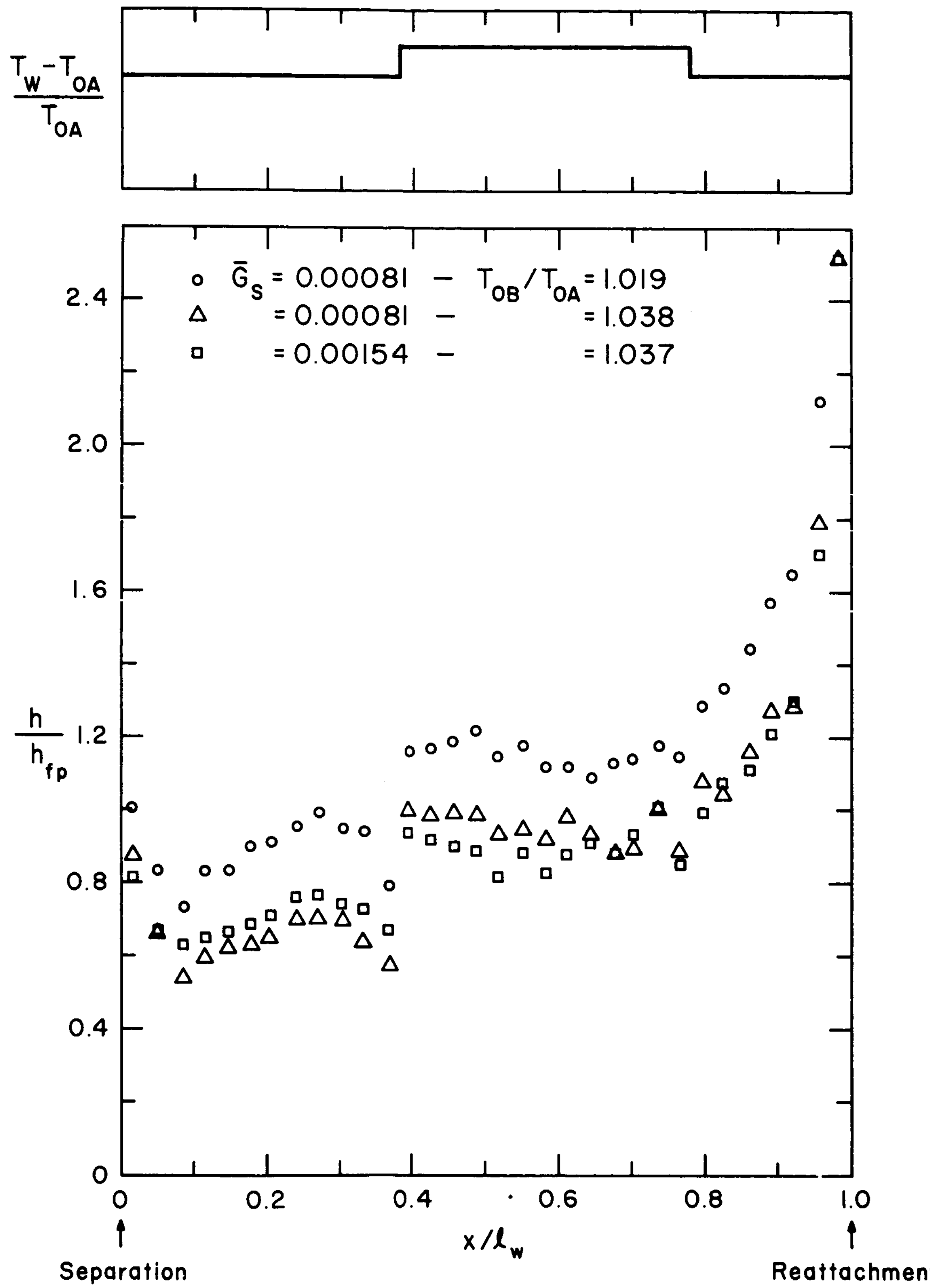

Figure 20. Local Heat Transfer Coefficient/Local Flat Plate Coefficient (Two-step Changes in Wall Temperature)

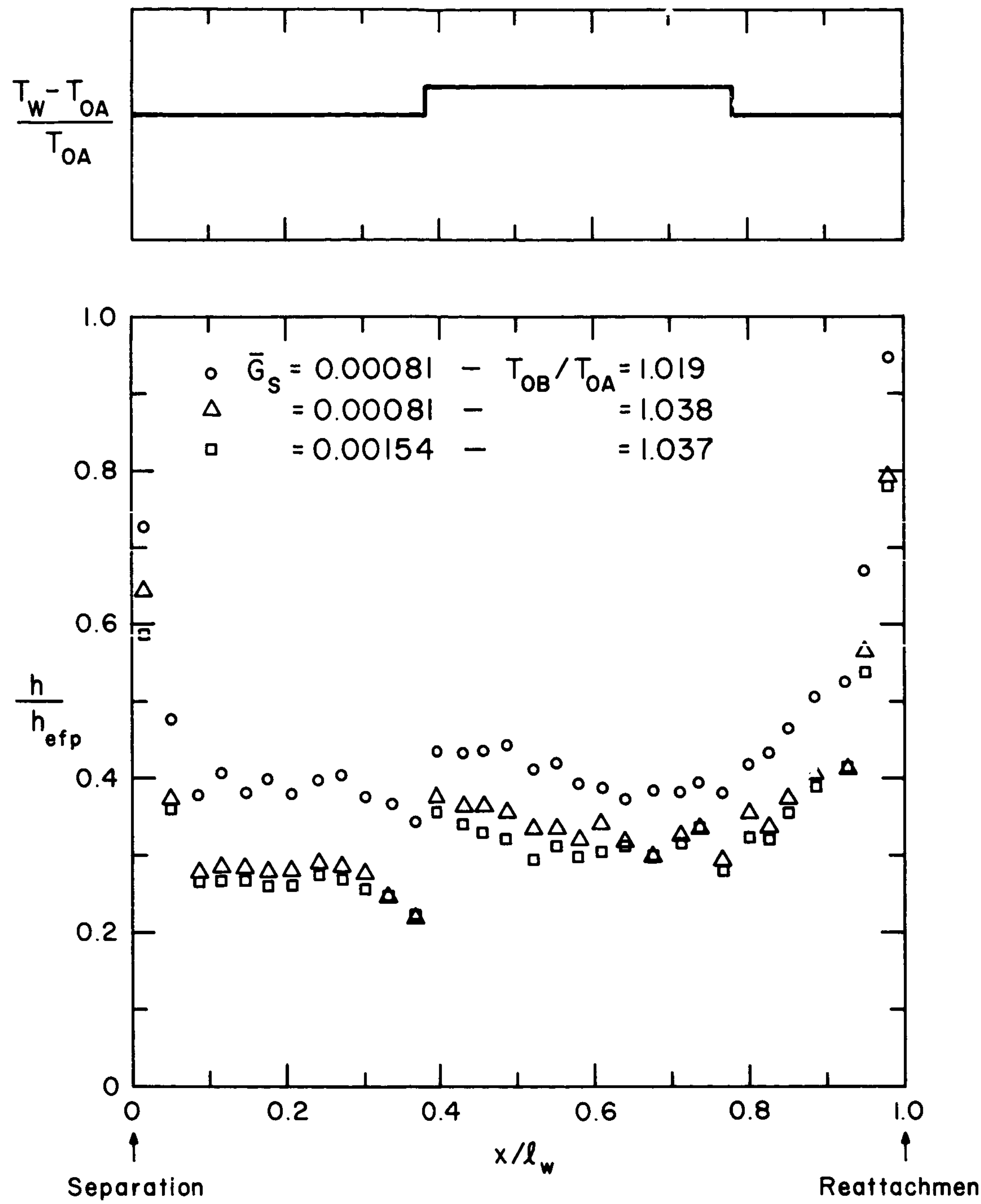

Figure 21. Local Heat Transfer Coefficient/Equivalent Mixing Length Flat Plate Coefficient (Two-step Changes in Wall Temperature)

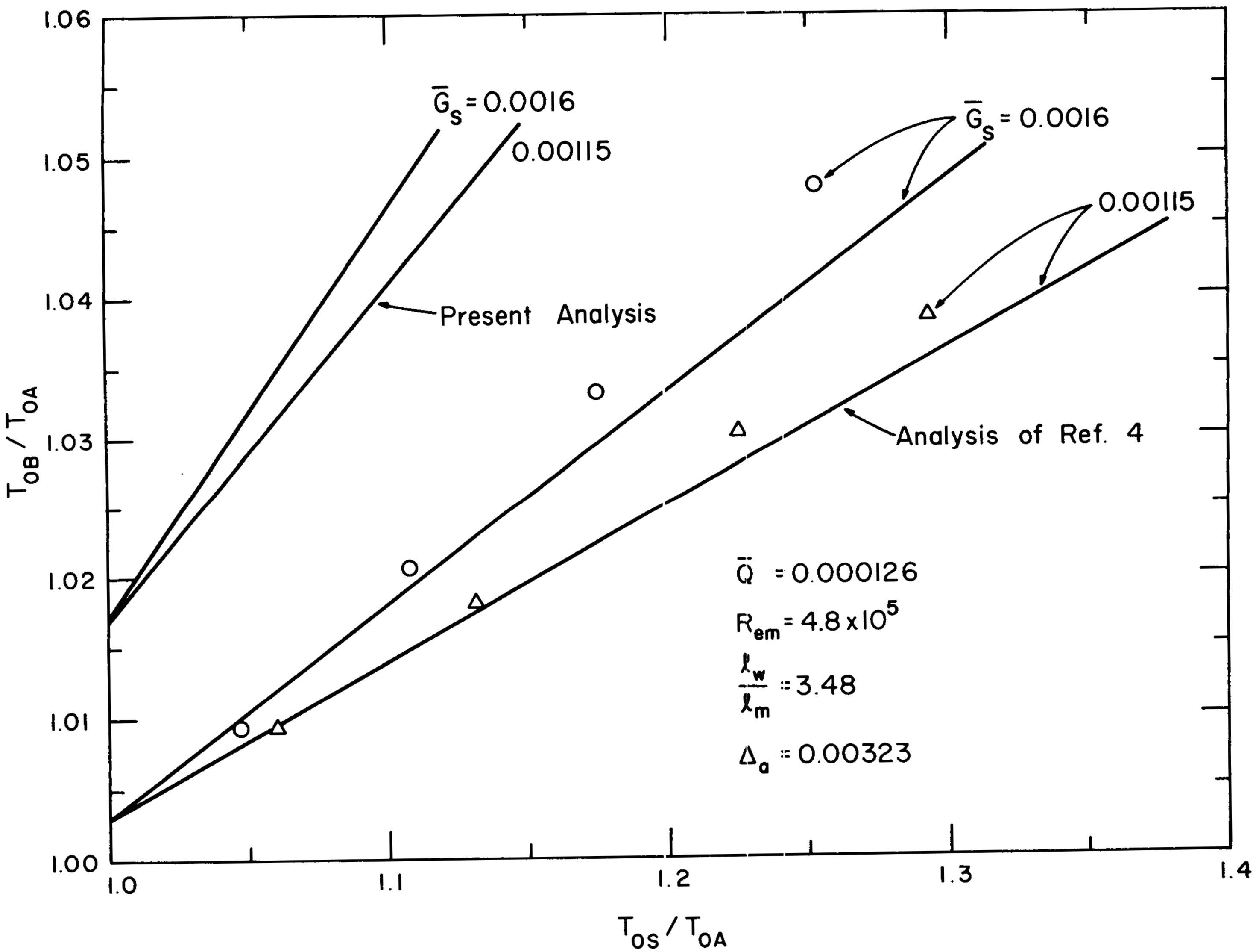

Figure 22. Bulk Temperature vs Bleed Temperature for Different Bleed Rates (Simulated Wall Heat Transfer)

REFERENCES

1. Korst, H. H., "Dynamics and Thermodynamics of Separated Flows," Agard Conference Proceedings, No. 4, Separated Flows Part 2, pp. 701-746, May 1, 1966.

2. Korst, H. H., and Chow, W. L., "Non-Isoenergetic Turbulent ($Pr_t = 1$) Jet Mixing Between Two Compressible Streams at Constant Pressure," Tn-393-2, Prepared under Grant No. NASA NsG-13-59 by University of Illinois, Urbana, Illinois. Also found in NASA CR-419, April, 1966.

3. Golik, R. J., "On the Dissipative Mechanisms Within Separated Flow Regions," Ph.D. Thesis, Department of Mechanical Engineering, University of Illinois, Urbana, Illinois, 1962.

4. Miles, J. B., "Stanton Number for Separated Turbulent Flow Past Relatively Deep Cavities," Ph.D. Thesis, Department of Mechanical Engineering, University of Illinois, Urbana, Illinois, 1963.

5. Kirk, F. N., "An Approximate Theory of Base Pressure in Two-Dimensional Flow at Supersonic Speeds," Royal Aircraft Establishment Tech. Note No. Aero 2377, December, 1959.

6. McDonald, H., "Turbulent Shear Layer Re-Attachment with Special Emphasis on the Base Pressure Problem," The Aeronautical Quarterly, Vol. 15, August, 1964.

7. Nash, J. F., "The Effect of an Initial Boundary Layer on the Development of a Turbulent Free Shear Layer," National Physical Laboratory, Aero report 101 9, June, 1962.

8. Lamb, J. P., "The Development of Free Turbulent Shear Layers," Aro. Inc., AEDC report No. TR-65-184, November, 1965.

9. Korst, H. H., Page, R. H., and Childs, M. E., "Compressible Two-Dimensional Jet Mixing at Constant Pressure," University of Illinois, ME-TN-392-1, OSR-TN-54-82, Contract No. AF 18(600)-392, April, 1954.

10. Pai, S. I., "Two Dimensional Mixing of a Compressible Fluid," Journal of Aero Sciences, Vol. 16, No. 8, pp. 463-469, 1949.

11. Yaffee, M. L., "Cavity Injection Explored for Hypersonic Cooling," Aviation Week and Space Technology, pp. 36-38, January 4, 1965.

12. Wu, J. C., "On the Finite Difference Solution of Laminar Boundary Layer Problems," Proceedings of the 1961 Heat Transfer and Fluid Mechanics Institute.

13. Reynolds, W. C., "Heat Transfer in the Turbulent Incompressible Boundary Layer with Constant and Variable Wall Temperature," Ph.D. Thesis, Department of Mechanical Engineering, Stanford University, Stanford, California, Sapt., 1957.

14. Larson, H. K., "Heat Transfer in Separated Flows," Journal of Aero/Space Sciences, November 1959.

15. Chapman, D. R., "A Theoretical Analysis of Heat Transfer in Regions of Separated Flow," NACATN 3792, Oct., 1956.

16. Charwat, A. F., Dewey, C. F., Roos, J. N., and Hitz, J. A., "An Investigation of Separated Flows - Part II: Flow in the Cavity and Heat Transfer." J. Aerospace Science, 28, 513, July 1961.

17. Fox, J., "Heat Transfer and Air Flow in a Transverse Rectangular Notch," Int. J. Heat and Mass Transfer, 8, 269, 1965.

18. Seban, R. A., "Heat Transfer and Flow in a Shallow Rectangular Cavity with Subsonic Trubulent Air Flow." To be published.

19. Nickerson, R. J., "Heat Transfer to Incompressible Boundary Layers," Developments in Heat Transfer, Ed. by W. M. Rohsenaw, 1964, MIT Press.

20. Kestin, J. and P. D. Richardson, "Heat Transfer Across Turbulent Incompressible Boundary Layers," Int. J. Heat and Mass Transfer, 6, 147, February 1963.

21. Spalding, D. B., "Heat Transfer to a Turbulent Stream from a Surface with a Step-Wise Discontinuity in Wall Temperature," Int. Developments in Heat Transfer: Part II, p. 439, 1961.

22. Spalding, D. B., "A Single Formula for the Law of the Wall," J. Applied Mechanics; Transactions of ASME, Series E, p. 455, 1961.

23. Hartnett, J. P., E. R. G. Eckert, R. Berkebak, and R. L. Sampson, "Simplified Procedures for the Calculation of Heat Transfer to Surfaces with Non-Uniform Temperatures," WADC Tech Report 56-373, December 1956.

24. Schlichting, H., "Boundary Layer Theory," McGraw-Hill Book Company, Inc.; Fourth Edition, 1960.

25. Peters, C. E., "A Model for the Free Turbulent Eddy Viscosity," Aro, Inc., report No. AEDC-TR-65-209, November 1965.

26. Pai, S. I., "Laminar Jet Mixing of Two Compressible Fluids with Heat Release," Jr. Aero Sciences, vol. 23, p. 1012-1018, November 1956.

27. Chow, W. L. and H. H. Korst, "On the Flow Structure within a Constant Pressure Compressible Turbulent Jet-Mixing Region," Department of Mechanical Engineering, University of Illinois, report No. ME-TN-393-1, July 1962.

28. Charwat, A. F., J. N. Roos, F. C. Dewey, and J. A. Hitz, "An Investigation of Separated Flows - Part I: The Pressure Field," Jr. of Aero-Space Sciences, vol. 28, No. 6, pp. 457-470, June 1, 1960.

29. Maull, D. J. and L. F. East, "Three-Dimensional Flow in Cavities," Jr. Fluid Mechanics, vol. 16, p. 620, 1963.

30. Jacob, M., "Heat Transfer," vol. II, John Wiley and Sons. Third Edition, 1957.

VITA

Ervin Lynn Bales was born February 21, 1932 in Des Moines, Iowa. He was reared and attended schools in Rock Island, Illinois.

He enlisted in the U. S. Marine Corps in August, 1949 and was discharged November, 1952. He attended the University of South Carolina until graduation with a Bachelor of Science in Mechanical Engineering in June, 1957.

He worked for United Aircraft Corporation, Research Department as a Research Engineer from graduation until January, 1960. He then moved to Caterpillar Tractor Company, Research Department as a Research Engineer until entering the University of Illinois in September, 1962. While at Caterpillar he attended night school at Bradley University and was awarded a Master's degree in Mechanical Engineering in June, 1962.

He has been a half-time assistant since entering the University of Illinois and has worked during three summers at Caterpillar Tractor Company.